

TOPICAL REVIEW

ELECTRON SPIN POLARIZATION ESP AT SURFACES OF FERROMAGNETIC METALS *

Carl RAU

Sektion Physik, University of Munich, Schellingstrasse 4, Munich 40, Fed. Rep. Germany

Received 4 March 1982; in revised form 28 June 1982

Fundamental information on surface magnetic order (SMO) of ferromagnetic metals can be obtained from electron-capture, photoemission, fieldemission, spin-dependent tunneling and spin-polarized LEED experiments. The different techniques, new experimental advances and developments are discussed with particular emphasis given to electron-capture spectroscopy. This review will focus on new experimental and theoretical results (long-range and "local" SMO of ferro- and antiferromagnetic metals, surface states, SMO of thin films, new magnetic surface phases, magnetic surface reconstruction, chemisorption) obtained in the years past which have brought outstanding progress towards a deeper comprehension of the physics of ferromagnetism and towards the unravelling of the physical processes inherently involved in the various methods for spin spectroscopy. Recent data on the SMO received from experiments performed at surfaces of single crystals of 3d-TM and 4f-RE metals reveal new scientific insights and perspectives for the theoretical analysis of experimental results within the framework of the currently refined knowledge about ferromagnetism.

Contents

1. Introduction	142	2.3.2. To the physics of the D ^o -atom: Production of deuterium nuclear spin polarization by ESP in the D ^o -electron shell . .	148
1.1. Introductory remarks and outline of the review	142	2.3.3. Adiabatic transition	149
1.2. Purpose of the review	143	2.3.4. T(d, n) ⁴ He-reaction	149
2. Physical basis and experimental technique of electron-capture spectroscopy (ECS) . .	143	2.4. Detection of ESP using two-electron capture	150
2.1. Introduction	143	2.5. Surface reflection of deuterons and scattering potential of the topmost atomic layer (probing depth of ECS in real space)	150
2.2. Experimental developments	144	2.6. Electron capture	152
2.2.1. Apparatus for ECS	144	2.7. Instrumentation for nonmagnetic surface analysis	152
2.2.2. Atomically clean and flat surfaces of single crystals	145	3. Research on 3d-transition and 4f-rare earth metals with ECS	153
2.3. Detection of electron spin polariza- tion (ESP) using one-electron cap- ture	146	3.1. Remarks on theoretical models and proposals on surface magnetism . . .	153
2.3.1. Formal description of electron spin polarization and deu- terium nuclear spin polariza- tion	146	3.2. Surfaces of 3d-transition metals: Ni, Co and Fe	154
		3.2.1. Ni(110), Ni(100), Ni(111), Ni(120)	155
		3.2.2. Co(0001), Co(10 $\bar{1}$ 0), Co(11 $\bar{2}$ 0) .	158
		3.2.3. Fe(110), Fe(100), Fe(111) . . .	159

* Supported by the Bundesministerium für Forschung und Technologie, Federal Republic of Germany.

3.3. Surface states: Ni(100)	160
3.4. Dependence of ESP on reflexion angle: Ni(110), Co(0001)	160
3.5. Ferromagnetism at surfaces of oligatomic, epitaxial Ni-layers: Ni(100)/Cu(100), Ni(100)/NaCl(100)	161
3.6. Search for magnetic surface phase transitions: Gd	163
3.7. H-chemisorption and ESP: Ni(110)	164
3.8. Surfaces of antiferromagnetic 3d-transition metals: Cr(100)	164
3.9. Local magnetic order and two-electron capture: Ni(110), Ni(100), Ni(111), Ni(120)	165
4. Results of further experimental techniques sensitive to ESP	166
4.1. Photoemission spectroscopy (PES)	167
4.2. Fieldemission spectroscopy (FES)	167
4.3. Spin-dependent tunneling in a superconductor-insulator-ferromagnet junction (SIFT)	168
4.4. Spin-polarized low-energy electron diffraction (SPLEED)	169
5. Summary and perspectives	169

1. Introduction

1.1. Introductory remarks on surface magnetism and outline of the review

Ferromagnetism has posed a fascinating challenge both to experimental and theoretical physicists for many decades. There is now an increasing interest in a deeper comprehension of ferromagnetism because of its pivotal importance in connection with surfaces. Ferromagnetic materials such as Fe, Co and Ni are widely used as commercial catalysts (cf. Fischer-Tropsch-processes, such as coal gasification and ethylene hydrogenolysis). The high, specific catalytic activity of these metals deteriorates by orders of magnitude due to changes in the magnetic structure caused by undesired surface reactions occurring at the topmost atomic layer alone. The investigation of the magnetic structure of surfaces of those materials is therefore

a prerequisite for a fundamental theoretical understanding of catalytical processes. Is the topmost atomic layer of a ferromagnetic material ferro- or paramagnetic? Questions of this kind have been discussed vehemently for many years. In diverse theoretical publications [1-3] it is shown that the magnetic structure of surfaces depends not only on the assumptions about the surface (lattice-structure, -relaxation and -reconstruction) but also drastically on the models of magnetism applied (i.e. molecular-field approximation, spin-wave approximation, etc.). Theoretical studies are primarily carried out for simple ordered structures, such as single crystalline surfaces. Therefore it is highly desirable to perform experiments also at well-defined and atomically clean surfaces of single crystals under ultra-high vacuum conditions. In general, bulk electronic properties of crystalline solids, which can be described by band-structure calculations, exhibit a crystallographic dependence caused by symmetry effects. For that reason surface electronic properties, likewise, exhibit a crystallographic dependence which, in principle, can be investigated by measurements using surfaces of single crystals.

For the analysis of surfaces of magnetic single crystals there is not only interest in data on the electronic densities of states as they are investigated, e.g., with conventional photoelectron spectroscopy, there is, in addition, to be added the sign and magnitude of the electron spin polarization (ESP) as a significant parameter for the characterization of the surface magnetic order (SMO) of ferromagnetic metals [4]. Information on SMO of ferromagnetic metals can be obtained from electron-capture, photoemission, fieldemission, spin-dependent tunneling and spin-polarized LEED experiments. We report on the various types of spectroscopies, new experimental advances and developments with particular emphasis given to electron-capture spectroscopy.

This review will focus on new experimental and theoretical results obtained in the past years which have brought outstanding progress towards a deeper comprehension of the physics of ferromagnetism, and towards the unravelling of the physical processes inherently involved in the various methods for spin spectroscopy.

In section 2 we present the physical basis and experimental technique of electron-capture spectroscopy (ECS). In section 3 we report on fundamental investigations with ECS on the ESP at single-crystalline surfaces of ferromagnetic and antiferromagnetic materials.

With ECS the SMO of atomically flat and clean surfaces of single crystals is investigated for the first time. Thereby new and surprising results were obtained which have highlighted the importance of single crystal measurements. Further ESP sensitive methods, recent experimental results, advances and developments are reviewed in section 4. In section 5 a summary is given, including promising areas of application for future progress of research in this vastly expanding field of surface physics.

1.2. Purpose of the review

In the past decade there has been an increasing scientific interest and activity in fundamental studies of the surfaces of magnetic metals. Several experimental techniques for *magnetic* surface analysis have been devised within this time. In several comprehensive reviews [5–9] various methods sensitive to ESP, experimental results, analyses and interpretations prior to the year 1976 were discussed. Further, in 1978, a detailed review [10] from a theoretical point of view, of the theoretical and experimental analyses of ESP in ferromagnetic metals was published. In this work new theoretical results for the interpretation of ESP data from fieldemission, photoemission and spin-dependent tunneling experiments were presented. Reviews of spin-polarized LEED from surfaces, including surfaces of ferromagnetic metals, have recently been published [11,12].

The aim of this review is not to give an extended description of the different ESP methods. For that purpose we refer the reader to the above mentioned reviews and original articles. We will limit ourselves to report on the various techniques – except ECS – insofar as necessary to comprehend the principle of each method by a wider community of readers.

We report on recent methodological and technological advances and developments as they relate to fundamental results which have brought

new scientific perspectives in both the field of surface physics and of magnetism.

2. Physical basis and experimental technique of electron-capture spectroscopy (ECS)

2.1. Introduction

ECS is a novel method to investigate ESP (section 2.3.1) at surfaces of magnetic single crystals under UHV conditions. The basic process of this method of spin spectroscopy is the capture of one or two spin-polarized electrons during small angle reflection of fast deuterons at single crystalline surfaces of magnetic crystals.

Fig. 1 illustrates an ion trajectory during reflection. For a reflection angle of 0.2° the ions interact approximately with a few hundred surface atoms. The minimum distance of the ions from the surface during the grazing angle reflection amounts to 0.2 nm (section 2.4), denoting that the ions interact in real space only with the exponential tail of the electronic wave functions at the surface. This fact determines the extreme surface sensitivity of ECS. The principle of the ECS experiment is shown in fig. 2.

2.1.1. Detection of ESP using one-electron capture (OEC) processes ($D^+ + e^- = D^0$)

A well collimated deuteron beam (half angle of divergence $< 0.025^\circ$) of 150 keV deuterons is reflected and thereby partially neutralized at a (*hkl*)-surface of a ferro- or antiferromagnetic single crystal magnetized to saturation parallel to the surface plane. After reflection the beam passes

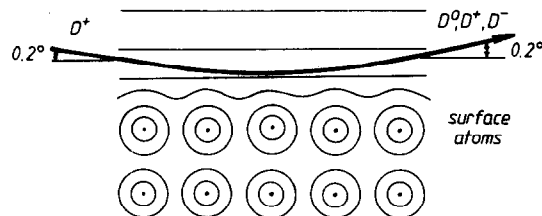


Fig. 1. Scheme of the ion trajectory for a reflection angle of 0.2° and surface potential plotted on a plane perpendicular to the reflecting surface.

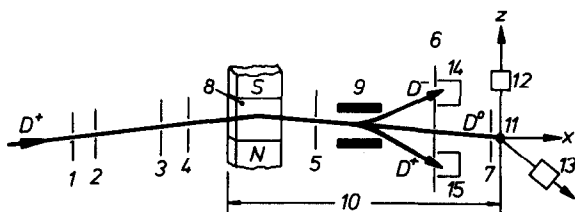


Fig. 2. Experimental arrangement: (1)–(7) ion beam collimating slits; (8) ferromagnetic target ($12 \times 8 \times 1.5 \text{ mm}^3$), magnetized perpendicular to the incoming beam direction; (9) electrostatic condenser; (10) weak magnetic field (0.8 mT), parallel to the target magnetizing field used as quantization axis (+z direction) in OEC experiments; (11) T-Ti-target; (12,13) Si surface-barrier solid-state detectors; (14,15) Faraday cups.

through an electric field to extract positive and negative charged ions. Therefore only neutralized particles impinge on a T-target (11 in fig. 2) and provide ^4He -particles via the $\text{T}(d, n)^4\text{He}$ -reaction. During an adiabatic transition from the high magnetic field region at the magnetic surface into a weak magnetic guiding field, part of the ESP in the electron shell of the neutralized atoms is converted into a nuclear polarization by hyperfine interaction. The nuclear polarization so achieved is determined via the T-reaction using the ^4He -count ratio $r = N_z/N_y$, in two Si-solid state detectors (12, 13 in fig. 2) and serves as a measure of the ESP (section 2.3) due to long-range SMO.

2.1.2. Detection of ESP using two-electron capture (TEC) processes ($D^+ + 2e^- = D^-$)

A well collimated beam of 100 keV deuterons is reflected at a demagnetized surface of a ferromagnetic single crystal. After reflection the beam passes through an electric field to split spatially the single charged positive and negative ions. The D^- and the D^+ ion currents are then simultaneously detected using two Faraday cups (14, 15 in fig. 2).

In section 2.4 we show that the charge state ratio $R = D^-/D^+$ (= D^- -fraction of the reflected beam/ D^+ -fraction of the reflected beam) is sensitive to the ESP due to "local" SMO existing on an atomic scale.

2.2. Experimental developments

Essential points during the exploration and experimental development of this method were the

design of a novel apparatus for surface reflection experiments (section 2.2.1) using ions as an atomic probe of the magnetic state of a surface and the planning of sensitive ESP-detectors (sections 2.3 and 2.4).

Further crucial points were the development of a technology to produce atomically clean and flat single-crystalline surfaces and the selection of methods suitable to analyze the chemical and geometrical structure of the topmost atomic layer of a surface (section 2.6).

First ECS results [13] revealed that the ESP depends on the respective orientation and on the cleanness of the surfaces showing that studies at well-defined (oriented, clean and flat) surfaces are a prerequisite for ESP studies. To achieve an extensive comprehension of surface magnetism it is necessary not only to investigate the ESP at surfaces of various magnetic materials but also to answer further fundamental questions (table 1) in surface magnetism, a fact which was a contributory determinant to the realization of the ECS apparatus.

2.2.1. Apparatus for ECS

Fig. 3 gives a schematic diagram of the apparatus used to study ESP at surfaces. It consists of a measuring chamber, a detection chamber for ESP,

Table 1
Particular questions connected with surface magnetism

Dependence of the ESP on temperature T	a) Sensitive test to check the applicability of different models for surface magnetism
	b) Check of models on the possible existence of ferromagnetic order beyond the bulk Curie temperature T_{Cb}
Influence of adsorbed impurity atoms on the ESP at surfaces	The introduction of localized states at clean surfaces allows to check models on chemisorption
ESP at surfaces of oligo-atomic epitaxial layers	Check of theoretical models on the possible existence of so-called "intrinsic magnetic dead layers"

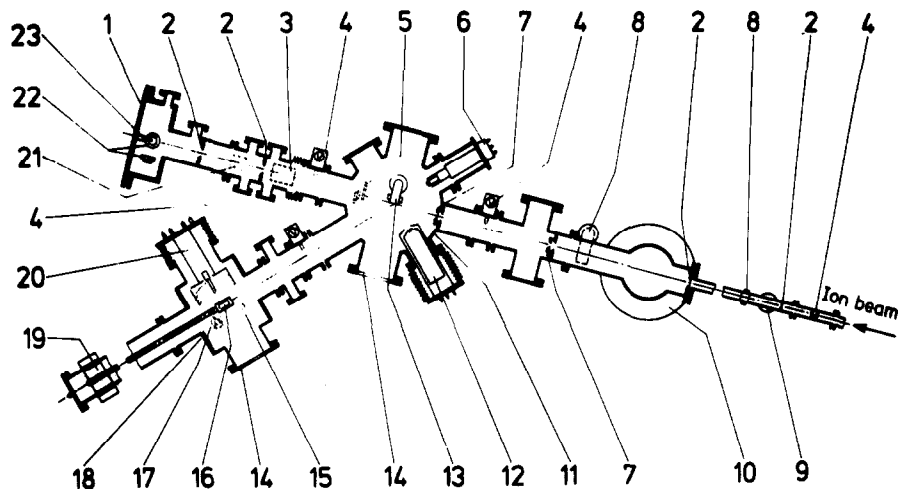


Fig. 3. Schematic diagram of the ECS apparatus: (1) chamber for detection of deuterium nuclear spin polarization; (2) slit; (3) deflector plates; (4) gate valve; (5) movable quartz screen and Faraday cup; (6) quadrupole mass analyzer; (7) movable slit; (8) bending magnet; (9) 25 l/s ion getter pump; (10) 150 l/s ion getter pump and liquid nitrogen cooled titanium sublimation pump; (11) target chamber with 400 l/s ion getter pump; 400 l/s turbo-molecular pump and 40000 l/s liquid nitrogen cooled titanium sublimation pump; (12) retractable Auger cylindrical mirror analyzer; (13) target manipulator with magnetizing coil, pole pieces and heating/cooling device; (14) window; (15) electron beam evaporation source; (16) target holder with heating device; (17) sputter ion gun; (18) chamber for target preparation with 400 l/s turbo-molecular pump and 10000 l/s liquid nitrogen cooled titanium sublimation pump; (19) linear and rotary drive; (20) retractable LEED/Auger 4-grid analyzer; (21) movable Faraday cups; (22) Si-surface barrier solid state detectors; (23) titanium-tritium target.

a chamber for specimen preparation and of a beam line and collimation system simultaneously used as pressure reducing system. This allows the ECS apparatus to be connected to an ion-beam accelerator operating at 10^{-7} mbar. Further details of the apparatus are given in the legend of fig. 3.

We present some important features and properties of the ECS apparatus:

1. The ESP measurements are performed in the target chamber (11) operating at a base pressure of 10^{-11} mbar, into which the specimens are transported in situ from the preparation chamber (18). C and O partial pressures are in the low 10^{-12} mbar region.

2. The ECS apparatus makes it possible to investigate the dependence of the ESP on temperature and on the magnetizing field.

3. The reflection angle is variable within an accuracy of 0.001° .

4. The ion beam collimating slits (2) are movable in two directions perpendicular to the incom-

ing beam direction with an accuracy of $5 \mu\text{m}$.

5. The angular acceptance of the ESP detectors (21,23) amounts to 0.05° .

6. The chemical and geometrical characterization of surfaces can be performed in situ with LEED and AES measurements (12, 20).

7. Oligatomic epitaxial magnetic layers can be produced at 10^{-10} mbar in a preparation chamber (18) by electron beam evaporation from cooled substrate materials.

8. Intensity and energy distributions, as well as neutralization probabilities of reflected ions, can be measured with an angular resolution of 0.001° , and with an energy resolution of 4 keV.

9. A well collimated (half angle of divergence $< 0.025^\circ$) energetic deuteron beam of high current density ($10 \mu\text{A}/\text{mm}^2$) helps to maintain clean surfaces over a long period of time (beam cleaning effect).

2.2.2. Atomically clean and flat surfaces of single crystals

The main emphasis for exploring surface pre-

paration techniques was concentrated on the production of single crystalline surfaces. Using polycrystalline surfaces for the measurement – even if the different surface orientations are present in statistical distribution – significant (*hkl*)-dependent information may be lost. The measurement then yields an average value for the ESP which makes the comparison with theoretical calculations of the ESP more difficult.

In theoretical investigations on the electronic states at surfaces primarily simple structures are investigated, e.g. atomically flat and infinite extended surfaces of single crystals. This extreme requirement naturally cannot be realized experimentally.

For ECS this requirement reduces to the condition that the regions of atomic flatness at the surface must be much larger than the lateral length of interaction (section 2.5) of the ion beam with the surface atoms. For a reflection angle of 0.2° the maximum interaction length amounts to a few hundred atomic distances requiring surface orientations better than 0.05° . Surfaces utilized for ECS experiments are prepared with an orientation better than 0.01° which is controlled using a precision X-ray spectrometer.

To characterize the flatness of a surface the “ion reflectivity” I (reflected ion beam intensity per solid angle/incoming ion beam intensity per solid angle) of a surface for 150 keV D^+ -ions is measured at a reflection angle of 0.2° . For the specimens used for ESP measurements I is always larger than 90%. Note that the interaction of the ion beam with the surface entails a surface flattening effect which increases I , too.

The pretreatment of all crystals consists of a mechanical polishing [14–16] of well-oriented surfaces with diamond powder down to a grain size of $0.1 \mu\text{m}$. The further treatment of the surfaces consists of a 5 h thermal annealing near the melting point of the material in hydrogen atmosphere. This treatment yields an additional flattening effect (thermal surface smoothing). This procedure (mechanical polishing/thermal annealing), which is also necessary for the crystal support used for thermal annealing, is repeated several times. In each cycle segregations of impurity atoms which, according to the high mobility of impurities at

high temperatures diffuse out of the bulk to the surface, are eliminated. For the characterization of magnetic single crystalline surfaces we utilize low-energy electron diffraction (LEED) (geometrical arrangement of surface atoms; see section 2.7), Auger-electron spectroscopy (AES) (chemical identity of surface atoms; see section 2.7), I (surface flatness; see also section 2.5) and ESP (magnetic order at the topmost atomic layer) measurements.

2.3. Detection of electron spin polarization ESP using one-electron capture (OEC)

The principle of the ECS method using OEC for the detection of ESP is simple: During reflection of 150 keV deuterons at surfaces of magnetized ferromagnetic materials, spin-polarized electrons are captured. The atomic part (D° -atoms) of the reflected beam then consists of D° -atoms polarized in electron spin. After reflection the beam then moves from the high magnetic field region proceeding along the whole target surface adiabatically into a weak magnetic guiding field (10 in fig. 2) where by hyperfine interaction a nuclear spin polarization in the D° -atoms is achieved serving as a measure of the original ESP of the captured electrons.

In the following we give a brief description of the polarization of spin 1/2 and spin 1 particles and report on some properties of the D° -atom which are important for the comprehension of this ESP-detector.

2.3.1. Formal description of electron spin polarization and deuterium nuclear spin polarization

Electron spin polarization. The spin polarization of electrons can be described by a polarization vector

$$\bar{P} = \{\langle \sigma_x \rangle, \langle \sigma_y \rangle, \langle \sigma_z \rangle\}; \quad (1)$$

using the expectation values of the well known Pauli spin matrices σ_x , σ_y , and σ_z [17]. (For spin 1/2 particles it is conventional to use the Pauli spin matrices σ_i ($\sigma_i = (2/\hbar)S_i$) instead of spin operators $S = (S_x, S_y, S_z)$.)

In the experiment only the component of \bar{P} along the direction of the macroscopic magnetization (parallel to the +z-axis; see fig. 2) is of importance (note that for electrons the spin moment is antiparallel to the magnetic moment). The degree P of the ESP along this axis is then

$$\begin{aligned}
 P &= P_z = \langle \sigma_z \rangle \\
 &= (n^+ - n^-)/(n^+ + n^-) \\
 &= n^+ - n^- \\
 &= 2n^+ - 1,
 \end{aligned}
 \tag{2}$$

with $-1 \leq P \leq +1$ and using $n^+ + n^- = 1$. n^- and n^+ represent the fractional expectation values for the occupation densities in an ensemble of electrons with spin moment parallel ($m_s = +1/2$) and antiparallel ($m_s = -1/2$), respectively to the +z-axis (see fig. 4).

P is a measure of the relative occupation densities for the two possible spin states of a spin 1/2 particle. The extreme values -1 and $+1$ correspond to an ensemble of electrons completely polarized parallel and antiparallel, respectively, to the +z-axis.

A target magnetizing field is applied to align

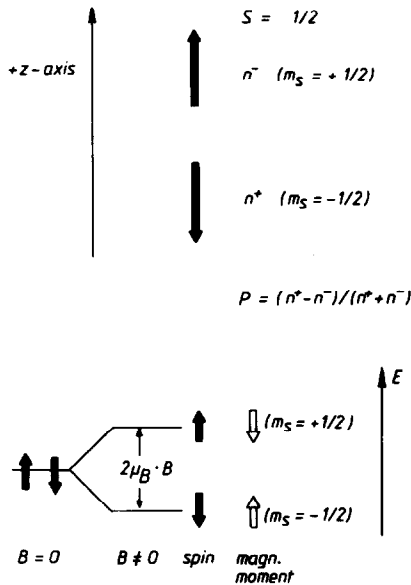


Fig. 4. Definition of ESP in solid state physics (upper part) and in atomic physics (lower part). B is the external magnetic field applied along the +z-axis (quantization axis).

randomly oriented Weiss domains thereby producing a macroscopic magnetization (long-range ferromagnetic order) which defines a preferred direction in space along which sign and magnitude of P can be measured.

Deuterium nuclear spin polarization The nuclear spin I of the deuterium atom is 1. The polarization of an ensemble of spin 1 particles can be described completely by its vector polarization \bar{P} and its Cartesian tensor polarization \mathbf{P}_{ij} which are commonly expressed by the expectation values of the Cartesian spin operators S_{ij} [18] which are (3×3) matrices:

$$\bar{P} = (1/\hbar)\{\langle S_x \rangle, \langle S_y \rangle, \langle S_z \rangle\},
 \tag{3}$$

$$\mathbf{P}_{ij} = (3/2\hbar^2)\{\langle S_i S_j \rangle + \langle S_j S_i \rangle - \delta_{ij}\}.
 \tag{4}$$

In the following we use a set of axes where the z-axis is used as quantization axis, a standard convention in nuclear physics since 1970 [19].

Fig. 5 gives a schematic representation of the 3 possible hyperfine substates $m_d = +1, 0, -1$ with their fractional populations N_{+1}, N_0, N_{-1} . By analogy with the vector polarization \bar{P} of spin 1/2

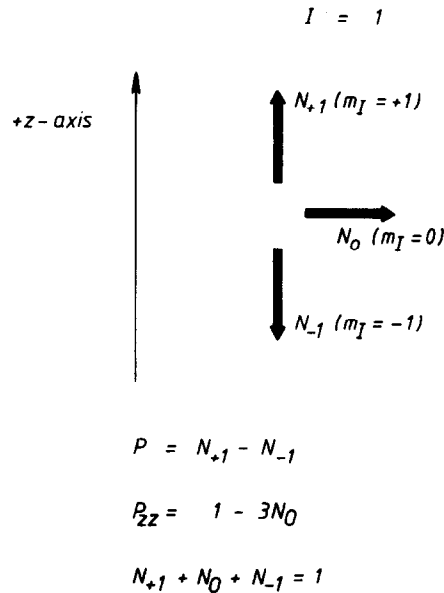


Fig. 5. Definition of deuterium nuclear spin polarization. The magnetic field direction is chosen along the +z-axis. (Note that for deuterons the magnetic moment is parallel to the spin moment.)

particles we then get for \bar{P} :

$$P_z = N_{+1} - N_{-1} \text{ and } P_y = P_x = 0, \quad (5)$$

with $N_{+1} + N_0 + N_{-1} = 1$. From eq. (5) we see that P_z depends only on N_{+1} and N_{-1} . The $m_d = 0$ projection does not contribute to the vector polarization, but contributes to the Cartesian components of the tensor polarization P_{ij} (eq. (4)):

$$\begin{aligned} P_{zz} &= 1 - 3N_0 = 3(N_{+1} - N_{-1}) - 2, \\ P_{xx} &= P_{yy} = (1/2)(3N_0 - 1), \\ P_{xy} &= P_{xz} = P_{yz} = 0. \end{aligned} \quad (6)$$

According to its definition the extreme values of P_{zz} are -2 and $+1$. The tensor component P_{zz} of a deuteron beam can be determined by measuring the angular distribution of ^4He -particles emitted in the $\text{T(d, n)}^4\text{He}$ -reaction (section 2.3.4).

In the next section we show under which experimental conditions P_{zz} is simply related to the ESP in the electron shell of D^0 -atoms.

2.3.2. To the physics of the D^0 -atom: Production of deuteron nuclear polarization by ESP in the D^0 electron shell

Fig. 6 gives the energy-level diagram for ground

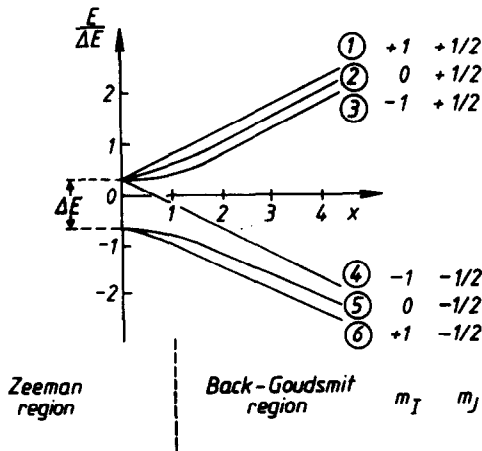


Fig. 6. Energy level diagram of the deuterium atom in an external normalized magnetic field $x = B/B_{cr}$ [20–22]. The energy is measured in units of $\Delta E = h \times 327.4 \text{ MHz} = 1.4 \times 10^{-6} \text{ eV}$ and the magnetic field is measured in units of $B_{cr} = \Delta E / (g_I - g_J)\mu_B$. For ground state deuterium B_{cr} amounts to 11.7 mT. (deuteron: $g_I = -0.47 \times 10^{-3}$; electron: $g_J = 2.002$; $\mu_B = -9.27 \times 10^{-24} \text{ J/T}$).

state ($^1\text{S}_{1/2}$) atomic deuterium ($I = 1, J = 1/2$) in a magnetic field [20–22]. The quantum numbers $m_d = m_I = +1, 0, -1$ and $m_s = m_J = +1/2, -1/2$ of each of the six hyperfine states, numbered (1–6), are shown in the right part of fig. 6. Note that for the high-energy hyperfine states (1–3) the spin moment of the electron is parallel (magnetic moment antiparallel) and for the hyperfine states (4–6) antiparallel, respectively, to the external magnetic field.

In high magnetic fields (see fig. 6, $x \gg 1$) electron spin and nuclear spin are decoupled causing an equal occupation of the hyperfine components with $m_d = +1, 0, -1$ which yields $N_{+1} = N_0 = N_{-1} = 1/3$ and therefore $P_{zz} = 0$. In the high field region an eventually existing ESP in the D^0 electron shells ($n^+ \neq n^-$, caused by capture of spin-polarized electrons) has no influence on the alignment of the nuclear spin states. By passing the beam (adiabatically) from the high field region into a weak field region ($x < 1$) where $F = I + J$ and $m_F = m_I + m_J$ are good quantum numbers and consequently the coupling between electron spin and nuclear spin is no longer negligible, a nuclear polarization can be achieved.

Fig. 7 gives the tensor component P_{zz} of a deuteron beam as function of a static applied external magnetic field if only one of the six possible

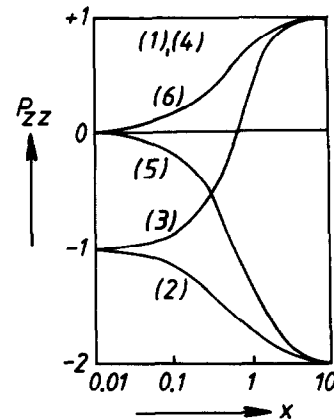


Fig. 7. Tensor polarization component P_{zz} of deuterons in deuterium atoms as function of an external normalized magnetic field x (see fig. 6) if one of the six possible hyperfine components (see fig. 6) in the deuterium atoms is occupied [20–22].

hyperfine components is occupied in the high field region [21,22]. From fig. 7 we see that the pure states (1) and (4) are independent of the external field, only states (2), (3), (5) and (6) depend on the external field. We simply derive from fig. 7 P_{zz} as function of n^+ (eq. (2)) in a weak external field ($x \approx 0$) by taking the weighted mean:

$$P_{zz} = (-1/3) + (2/3)n^+. \quad (7)$$

Applying eq. (2) yields for the ESP in the D° -atom

$$\bar{P} = +3P_{zz}. \quad (8)$$

Note that eq. (8) only holds if the neutralization of the deuterons takes place in a high magnetic field regime – requiring for capture of an electron into the ground state of deuterium a magnetic field larger than 11.7 mT ($x = 1$) – and if the adiabaticity (section 2.3.3) of the transition from “high” to “low” fields is guaranteed. We also note that the nuclear alignment is solely generated by the interaction between the deuterium nucleus and the magnetic field $B_J(0)$ produced by the captured electron at the nucleus site which amounts to 17.4 T for a ground state electron [21]. There is no alignment of the deuterons by magnetic interaction with the magnetic field at the surface of the ferromagnetic specimens [23].

2.3.3. Adiabatic transition

In the high magnetic field region $B \gg B_{cr}$ ($= 11.7$ mT) the interaction energy of the magnetic moment μ_I ($= 4.36 \times 10^{-27}$ J/T) of a deuteron with the magnetic field $B_J(0)$ of the electron at the nucleus site is smaller than the interaction energy of the total magnetic moment μ_{atom} of the deuterium atom with the external field B yielding

$$\mu_I B_J(0) \ll |\mu_{atom} B|, \quad (9)$$

which means that nuclear spin I and electron spin J are decoupled. Consequently, an ESP in the electron shell of the D° atom then has no influence on the occupation densities of the nuclear spin states.

During the transition into the Zeeman-region this coupling is no longer negligible and an alignment of the nuclear spin states in the field $B_J(0)$ takes place. The adiabaticity of this transition is

guaranteed if the change of the magnetic field energy of the deuterium atom during the decrease of the external field and during one Larmor period w_L^{-1} is always smaller than the smallest energy difference ΔE between two hyperfine states [24,25]. We then get

$$|w_L^{-1} \text{d}/\text{d}t(\mu_B B)| \ll \Delta E. \quad (10)$$

With $w_L^{-1} = \hbar/\mu_B B$, $\Delta E = -g_J \mu_B B/(I + 1/2) = -(2/3)(\mu_B B)$ and $\text{d}t = \text{d}z/v_D$ (velocity of 150 keV D° -atoms: $v_D = 3.8 \times 10^6$ m/s) we yield for the magnetic field gradient the following inequality

$$\begin{aligned} \text{d}B/\text{d}z &\ll (2/3)(\mu_B/\hbar v_D)B^2 \\ &\ll 0.015B^2(1/\text{mT mm}). \end{aligned} \quad (11)$$

For the critical field region $B_{cr} \approx 10$ mT we yield $\text{d}B/\text{d}z \ll 1.5$ mT mm. If this criterion (eq. (11)) is fulfilled then eq. (8) can be used to calculate the ESP in the D° -electron shell from the tensor component P_{zz} of the nuclear spin polarization.

2.3.4. $T(d, n)^4\text{He}$ -reaction

The $T(d, n)^4\text{He}$ -reaction with a Q -value of 17.56 MeV is commonly known as source for fast (14 MeV) neutrons [26,27]. For deuteron energies below 300 keV this reaction is preferentially suitable for analyzing the tensor polarization of deuterons. At a deuteron energy of 107 keV there exists a broad (140 keV) S-wave resonance of high efficiency (5 b) [28,29], which is solely due to the $J = (3/2)^+$ -niveau of the ^5He -compound nucleus. Applying an unpolarized deuteron beam for the $T(d, n)^4\text{He}$ -reaction yields an angular distribution of the emitted ^4He -particles, which is isotropic in the cms. Above 200 keV only, the differential cross section shows a weak anisotropy which is caused by a contribution of higher partial waves and in addition by a contribution of S-waves with $J = (1/2)^+$ [30–33]. Goldfarb [34] has shown that the differential cross section $\sigma(\alpha)$ in the energy region of this resonance depends only on the tensor polarization component $P_{zz} (= 1 - 3N_0)$ parallel to the applied magnetic field:

$$\sigma(\alpha) = \sigma_0 \left(1 - \frac{1}{4}(3 \cos^2 \alpha - 1)P_{zz}\right). \quad (12)$$

σ_0 is the unpolarized differential cross section of

this reaction and α is the angle between the z -axis and the direction of emission of the ^4He -particles. Applying polarized deuterons therefore yields an anisotropic distribution of the ^4He -particles. Maximum sensitivity is given for $\alpha = 0^\circ$ and $\alpha = 90^\circ$. With N being the respective ^4He count-rates we yield for the anisotropy factor r

$$r = (N_z/N_y) = \sigma(\alpha = 0^\circ)/\sigma(\alpha = 90^\circ) \quad (13)$$

or

$$P_{zz} = 4(1 - r)/(r + 2). \quad (14)$$

With eq. (8) we get for the ESP

$$P = +3P_{zz} = 12(1 - r)/(r + 2). \quad (15)$$

The maximum count ratio (1.273) is related to an ESP of -100% and the minimum count ratio (0.769) is related to an ESP of $+100\%$. The energy of the emitted ^4He particles amounts to 3.5 MeV which can be easily measured by aid of Si-surface-barrier solid-state detectors.

2.4. Detection of ESP using two-electron capture (TEC)

Contrary to OEC, which can be used to investigate long-range SMO at surfaces, TEC can be utilized to detect "local" SMO at surfaces on a microscopic scale. The basic idea for the TEC experiment depends on the fact that TEC processes predominantly occur within one single magnetic domain. The lateral length of interaction of a deuteron with the reflecting surface is only a few hundred atomic distances, which is much smaller than the lateral dimensions (μm - mm) of ferromagnetic domains. Two electrons captured by a single deuteron therefore possess the same spin alignment given by the direction of the spontaneous ferromagnetic order existing in each domain even in demagnetized samples. Two electrons in a domain are aligned either parallel or antiparallel corresponding to a triplet or singlet final state in a formed D^- -ion.

Using deuterons (or protons) for TEC we note that for D^- -ions only singlet- $1s^2$ -states exist. Stable triplet states such as $\text{D}^-(1s2s)$ with two electrons with spin aligned parallel do not exist

[35–37]. Consequently, the formation of D^- -ions is drastically suppressed employing ferromagnetic surfaces with an ESP of $+100\%$ or -100% . Using surfaces of nonmagnetic materials such as Cu where the electrons are nonpolarized the formation of D^- -ions is not suppressed.

At present, no theoretical treatment of D^- formation and survival during surface reflection of high energy deuterons is available [38]. Therefore, in a first approximation [39], we relate the measured charge state ratio $R = \text{D}^-/\text{D}^+$ at Ni and Cu surfaces directly to the corresponding fractional numbers n_{Ni} and n_{Cu} for Ni and Cu surfaces

$$R_{\text{Ni}}/R_{\text{Cu}} = n_{\text{Ni}}/n_{\text{Cu}}. \quad (16)$$

With $P = 0$ for Cu and $n_{\text{Cu}}^+ + n_{\text{Cu}}^- = 1$ we get from eq. (2) $n_{\text{Cu}}^+ = n_{\text{Cu}}^- = n_{\text{Cu}} = 0.5$. For Ni the negative ion formation rate determining fractional electron number is $n_{\text{Ni}} = (1 - |P|)/2$ with $n_{\text{Ni}}^+ + n_{\text{Ni}}^- = 1$. We then yield for P :

$$|P_{\text{Ni}}| = 1 - (R_{\text{Ni}}/R_{\text{Cu}}). \quad (17)$$

Note that spin-flip processes between the negative ions and the solid are negligible because the particles interact only for a time of 10^{-14} s in the close vicinity of the surface whereas spin-flip processes occur in a time scale of 10^{-12} s [40].

2.5. Surface reflection of deuterons and scattering potential of the topmost atomic layer (probing depth of ECS)

First ion-surface reflection experiments with 150 keV deuterons at single crystal surfaces revealed that for small scattering angles (0.2° – 0.8°) the ions are scattered specularly. From fig. 8 we see that the energy distribution of the ion beam changes insignificantly by the surface reflection, a fact which is characteristic for ion-reflection at surfaces of atomically flat single crystals. The angular divergence of the incident deuteron beam of 150 keV amounts to 0.05° . After the reflection at the single crystalline surface the charge-split parts of the scattered beam impinge on a T-Ti-target (11 in fig. 2; OEC experiment) and on two Faraday cups (14 and 15 in fig. 2; TEC experiment) for the measurement of the long-range and "local" SMO. The angular acceptance of the T-target and

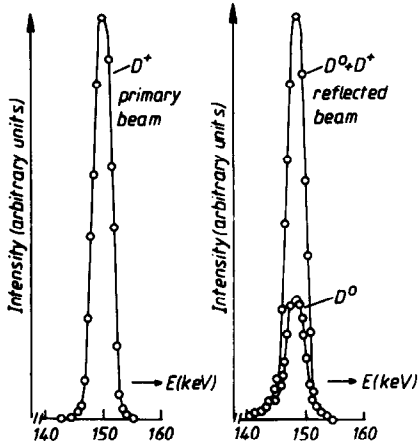


Fig. 8. Particle-energy distributions for 0.2° -grazing angle reflection of 150 keV deuterons at a Ni(110) surface.

of the two Faraday cups equally amounts to 0.05° guaranteeing that only optimally reflected particles are utilized in the measurements. Replacing the T-target and the Faraday cups by cooled Si-surface-barrier solid-state detectors with an angular acceptance of 0.05° allows the measurement of the “ion reflectivity” I , which, for well-prepared specimens, is always larger than 90%. This procedure allows the detection of the SMO existing in the atomically flat parts of the surfaces of the investigated crystals. We remark that particles which are scattered at atomic steps at the surface are emitted with larger angles than the angle of incidence. ECS experiments utilizing these particles for the ESP measurements always yield lower ESP values compared to the ESP values due to the SMO existing at the atomically flat parts of the surfaces. For very small angles of incidence ($\approx 0.2^\circ$ – 0.8°) the ions interact only with a few hundred atoms along the topmost surface layer.

At present from literature there are two different concepts available to describe the ion-surface interaction in this regime:

1. The scattering is treated as a sum of individual ion-atom collisions. This concept allows the simulation of realistic surfaces (allowance for anisotropic thermal lattice vibrations and for irregularities in the periodic arrangement of the surface atoms).

2. The scattering of the atoms of the topmost atomic layer is treated using a one-dimensional, static and continuous, repulsive interaction potential [41–43]. This concept is suitable for the computer simulation of high-energy ion-reflection at atomically flat surfaces.

The second concept is quite useful in calculating the distance d_{\min} of the closest approach of the ions towards the reflecting surface. d_{\min} is well characterized by the energy component E_{\perp} of the ions normal to the surface

$$E_{\perp} = E_0 \sin^2 \alpha \approx E_0 \alpha^2. \quad (18)$$

With $E_0 = 150$ keV, E_{\perp} amounts to 1.8 eV for a reflection angle $\alpha = 0.2^\circ$. For the estimation of d_{\min} we use a planar surface potential derived from a superposition of screened Coulomb potentials of the Thomas–Fermi type [44,45] with the screening function of Molière [46]. Fig. 9 gives a plot of these potentials for D^+ -reflection at Ni(110) and Co(0001) surfaces. From these potentials we estimate $d_{\min} \approx 0.2$ nm for $\alpha = 0.2^\circ$. This

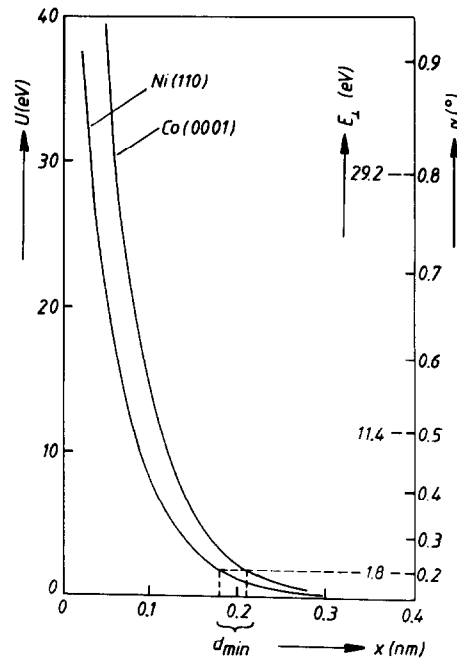


Fig. 9. Thomas–Fermi–Molière surface potentials $U(x)$ for reflection of 150 keV deuterons at Ni(110) and Co(0001); x = distance from the surface in nm.

fact clearly reveals that the ions interact solely with the exponential tail of the electron density at the surface. Note that this estimation of d_{\min} is only an approximation in the frame of the validity of these potentials shown in fig. 9. At present there is no calculation available where the ion reflection at ferromagnetic surfaces is treated using dynamic, self-consistent and spin-polarized surface potentials.

2.6. *Electron capture*

Of recent years several theories concerning electron capture have been published, essentially to calculate the neutralization probability of protons traversing thin metallic films [47–49]. Does the neutralization of protons or deuterons occur inside the material or only at the exit surface?

This question has become a test for the applicability of all theories. It is strongly correlated to the problem of the possible existence of bound states of a proton inside the solid. Brandt and Sizmann [47] in their theory reach the conclusion that for a proton at any velocity there exists no stable bound state inside the solid. Due to the collective screening of the proton charge by conduction electrons the energy levels of the proton are shifted in energy up to or above the Fermi level, not allowing the formation of neutrals until the particles have reached the tail of the electron density at the exit surface [48].

Cross [49] calculates the charge states of fast protons during transmission through solids visualizing charge exchange as a sequence of electron-capture and -loss processes into bound states of the proton. In this theory the existence of a surface plays no special role. The charge state equilibrium already exists inside the material. According to Cross the mean free path for electron-loss amounts to approximately 0.3 nm for 100 keV protons.

Ohtsuki and coworkers [50] calculate the neutralization probability for protons assuming that the electron-capture solely takes place at the exit surface. In a further paper [51] by these authors the neutralization of slow protons during scattering at a solid surface is treated assuming that only

Fermi electrons with a k vector normal to the surface are captured.

A theory on the k -vector selection for electron capture during ion scattering at metal surfaces has been published by Schröder [52] in the frame of the free electron model. He finds that the most energetic electrons (Fermi electrons) with k -direction in a forward cone between surface normal and projectile velocity are favoured for capture. In this paper it is further shown that high particle velocities ($v > 1.5$ au) or large d_{\min} values (corresponding to small reflection angles; see section 2.5) rotate the most favoured k -vectors towards the surface normal in qualitative agreement, with the assumptions used for the interpretation of ECS results (see section 3.2.1).

Further theories on electron-capture are reviewed in the paper by Cross [49]. Cross and Schröder in their work point out that tractable and realistic surface wave functions must be available for refined calculations on electron-capture in small-angle ion-surface reflection experiments.

For the interpretation of ECS results we assume – in a first approximation – that the deuterons directly probe the spin-polarized electron densities in the exponential tail of the electronic wave functions at the surface.

In this approximation we leave aside any effects such as an occupational disturbance of the spin-up and spin-down electron densities at the surface caused by Coulomb interaction of the reflecting ions with the solid or spin flip effects between the neutralized deuterium atoms and the solid. It is the velocity of the reflecting deuterons which allows us to describe the dynamical polarization of the electrons in terms of linear response considerations where no perturbation effects of relative electron spin densities are expected. Possible spin-dependent perturbations induced by the dynamical interaction of the ion with the solid cannot be efficient because the electronic response lags a few Å behind the swift ions [53,48,49].

2.7. *Instrumentation for nonmagnetic surface analysis*

With ECS the SMO at the topmost atomic layer of a solid can be investigated. For the nonmag-

netic surface analysis, therefore, only methods can be used which allow the characterization of the geometrical and chemical arrangement of the atoms in the topmost surface layer excluding all classical techniques for solid-state analysis (X-ray diffraction, neutron activation analysis, Mikrosonde, etc.).

The installation of analytical techniques of high surface sensitivity is not only required for the interpretation of ECS results, it is also necessary for checking the efficiency of new methods for the production of atomically flat and clean single-crystalline surfaces, of oligatomic epitaxial magnetic films or single-crystalline surfaces with well-defined contamination layers.

For the investigation of the periodic arrangement of surface atoms we utilize low-energy electron diffraction (LEED) measurements, which yield information about the lattice structure of the topmost atomic layers of a surface [54].

For the chemical analysis of the topmost atomic layers we utilize Auger-electron spectroscopy (AES) [55], which is sensitive to 1/1000 of a monolayer within an information depth of 0.4–2 nm for electron energies between 50 and 1000 eV [56]. Unfortunately at present one cannot derive from AES measurements the spatial distribution of impurity atoms in these topmost atomic layers. An important feature of AES is the sensitivity to the chemical bonding of surface atoms (chemical shift and splitting of AES “peaks”).

From ECS measurements at uncleaned, oxygen covered Gd surfaces it is found that the SMO depends on the chemical state of the O and Gd atoms at the surface. Using a movable cylindrical mirror analyser (CMA) for AES, changes in the shape and position of Gd-, GdO- and O-“peaks” caused by a step by step oxidation [57,58] of the surface can be correlated to changes in the ESP during the measurement.

3. Research on 3d-transition and 4f-rare earth metals with ECS

3.1. Remarks on theoretical models and proposals on surface magnetism

The present situation and the current comprehension of 3d- and 4f-bulk and surface ferromag-

netism is marked out by an extensive literature and by a continuous increase of theoretical and experimental investigations. In the last ten years a plurality of ESP experiments at surfaces of magnetic materials have been performed revealing that ESP measurements provide valuable and profitable information for the identification of the magnetic structure of a solid [59–62].

At present there exists no universal and unified theory to describe the magnetic structure of a solid. Already for the description of the ground state properties of a ferromagnetic material drastic model assumptions – initiated by Heisenberg [63], Bloch [64], Slater [65] and Stoner [66] – must be made. The 2 most frequent models are:

1. The Heisenberg model [63]: In this model electrons responsible for ferromagnetism are localized in real space at the position of the lattice atoms. The interaction between these localized electrons is produced by the interatomic exchange interaction which generates a spontaneous magnetic moment in the ground state. A typical difficulty of the Heisenberg model is that it does not account for the “metallic” properties – such as electrical conductivity – of the 3d-transition and the 4f-rare earth metals.

2. The Bloch model [64]: In this model electrons are localized in k -space within a few eV near the Fermi level. Specific ferromagnetic properties of the individual metals are then traced to differences in the one-electron energy structure existing in k -space.

Using the hypothesis of an “inner molecular field” – postulated by Weiss [67], Slater [65], Stoner [66] and Wohlfarth [68] – showed in the frame of the band model that for the 3d-transition metals Fe, Co and Ni the spin degeneracy can be partially removed by this “inner molecular field”. This fictive field then generates the ferromagnetic coupling between the conduction electrons giving rise to a spontaneous magnetic moment in the ground state of these metals. The main contribution to the spontaneous magnetic moment in these metals originates from electrons near (1–2 eV) the Fermi level which, dependent on their band character (3d-like, 4s-like) and on their k -vector, exhibit the well-known ferromagnetic exchange splitting.

The main difficulty of the Bloch model, also named SWS-model – after Slater, Stoner and Wohlfahrt – or “itinerant-electron” model, consists in the explanation of the physical origin of this “inner molecular field”. According to Slater [65] and Friedel [69] the intra-atomic exchange interaction, which is also responsible for Hund’s rule, generates ferromagnetic behaviour in the transition metals. After Kanamori [70], Hubbard [71] and Gutzwiller [4] the correlation energy, which is the repulsive Coulomb interaction between electrons with antiparallel spins, causes ferromagnetism in the transition metals.

In addition to these two limiting models there are recent theoretical efforts to reconcile these mutually opposite models into a unified one which could cover the entire field of magnetism [72,73]. Unfortunately, at present, there exists no calculation of the temperature dependence of ferromagnetic properties of the 3d-transition metals in the frame of band-structure calculations.

Are there modifications in the magnetic structure of infinite extended materials by the introduction of a surface?

For a surface atom the number of nearest neighbours is reduced compared to a bulk atom, a fact which could produce changes in the magnetic structure of materials where the Heisenberg model is more appropriate. Moreover, at the surface the symmetry properties of the crystal lattice are changed, a fact which in addition could lead to drastic changes in the magnetic order at the surface caused by surface states.

One may ask: Are there *drastic* perturbations in the magnetic structure at the surface of ferro-, antiferro- and paramagnetic materials to be expected or exists at surfaces – leaving aside small modifications – the magnetic structure of the infinite extended crystal since the surface region is only a small region of the total solid and cannot drastically affect the electronic and magnetic properties of Bloch electrons in the ground state? At present questions of this kind are discussed vehemently.

For the case of 3d-transition metal surfaces there exist the following model-dependent proposals:

1. Under the assumption that the ferromagnetic exchange splitting in the first approximation is not changed, no drastic changes in the magnetic structure are expected going from the bulk to the surface: Desjonquères and Cyrot-Lackmann [74].

2. Due to the local character of the “renormalized-atom approach” model drastic changes in the magnetic structure are expected going from the bulk to the surface. It is suggested that spin-dependent surface resonances can cause a change in the sign of the ESP at a Ni(100) surface: Fulde, Luther and Watson [75–77]. In this work the existence of so-called “intrinsic magnetic dead layers” at Ni surfaces is also discussed.

For the surface of the 4f-metal Gd there exist the following proposals: Leaving aside Friedel oscillations there are only small (10^{-3}) changes in the magnetic structure going from the bulk to the surface: Kautz and Schwartz [78]. (In this work the magnetization of the localized 4f-electrons is treated in the Heisenberg model. The magnetization of the conduction electrons is treated self-consistently. Changes in the temperature behaviour of the magnetic structure going from the bulk to the surface are possible.) In the frame of one-electron band structure calculations for antiferromagnetic materials such as Cr and V possessing an extreme high paramagnetic susceptibility, a ferromagnetic surface layer is expected: Allan [79].

In the following we present experimental results on the ESP using ECS at surfaces of ferro- and antiferromagnetic metals.

3.2. Surfaces of 3d-transition metals: Ni, Co and Fe

Table 2 gives results for the ESP results detected with ECS using OEC at the topmost atomic layer of Ni, Co and Fe single crystals. A striking and fundamental finding of these ECS experiments is that the ESP depends with respect to sign and magnitude on the surface orientation (*hkl*) demonstrating the importance of measuring ESP as function of the crystallographic surface indices.

In these measurements the reflection angle of the 150 keV deuterons amounts to 0.2° giving a distance of closest approach of the ions towards the reflecting surfaces of approximately 0.2 nm

Table 2
Electron spin polarization P measured at room temperature with ECS using OEC at fcc-Ni, hcp-Co and bcc-Fe surfaces

	Reflection plane (hkl)	Beam direction $u^v w$	Direction of magnetic field	$P(hkl)$ (%)		(Refs.)
				experiment	band structures	
Ni (fcc)	110	$\bar{1}12$	$\bar{1}11$	-96 ± 3	-65 to -100	[81-90]
	100	012	$0\bar{2}1$	-65 ± 1	-75 to -100	[81-90]
	100	001	010	-64 ± 1		
	111	$\bar{1}\bar{1}0$	$1\bar{1}\bar{2}$	-44 ± 2	-40 to -100	[81-90]
	120	001	210	$+15 \pm 1$	+17	[88]
Co (hcp)	120	$\bar{2}10$	001	$+16 \pm 1$		
	$10\bar{1}0$	0001	$\bar{1}\bar{2}10$	$+33 \pm 3$	+40 to -90	[91-93]
	$11\bar{2}0$	0001	$\bar{1}\bar{1}00$	$+27 \pm 3$	-80 to -90	[91-93]
Fe (bcc)	0001	$10\bar{1}0$	$\bar{1}\bar{1}00$	-41 ± 2	-50 to -100	[91-93]
	111	$\bar{1}\bar{1}\bar{2}$	$\bar{1}\bar{1}0$	$+31 \pm 2^a$	-15 to -40	[94-98]
	100	001	010	$+14 \pm 2^a$	+50 to -50	[94-98]
	110	$\bar{1}\bar{1}0$	001	$+13 \pm 2$	+15 to -45	[94-98]

^a Measured at 250°C.

(section 2.5). These ESP data therefore are attributed to the interaction of the ions with the spin-polarized electron states in the exponential tail of the electronic wave functions at the surfaces.

From table 2 we derive that the ESP does not depend on the azimuthal direction of the incoming beam. It is only a characteristic of the surface orientation (cf. Ni(100) and Ni(120) in table 2).

We further find P unequal to zero at all Ni, Co and Fe surfaces indicating the absence of ferromagnetic dead layers at clean Ni, Co and Fe surfaces and suggesting the inapplicability of theoretical models where the possible existence of "intrinsic magnetic dead layers" is discussed [75-77]. In section 3.7 we show that so-called "intrinsic magnetic dead layers" can be simulated at a (previously) ferromagnetic surface by H-contamination.

In the following we restrict ourselves to an interpretation of ESP results detected at 3d-transition metal surfaces in the frame of the band-theoretical description of the magnetic structure of these metals which allows the calculation of the dependence of the ESP as a function of surface orientation.

At present - leaving aside first calculations for Ni(100)-surfaces [80] (see section 3.3) - there are

no self-consistent, spin-polarized surface band-structure calculations for the ferromagnetic 3d-transition metals available: Therefore in the following we check to see if a quantitative or at least a qualitative interpretation of ECS results at 3d-transition metal surfaces is possible in the frame of self-consistent ferromagnetic one-electron band-structure calculations for infinitely extended materials published so far. The possible influence of surface states on the SMO is discussed in section 3.3.

3.2.1. Nickel

Within the 3d-ferromagnetic metals Ni is the most detailed investigated material and is the center of the classical controversy in literature concerning the applicability of the SSW-model for the description of ferromagnetism in the transition metals.

In fig. 10 spin-polarized total electron densities for Ni are shown as function of electron energy.

An essential feature of the SSW-model for Ni is the existence of incompletely filled 3d-bands with high electron densities of state near the Fermi level.

The following criteria are characteristic for the SSW-model for Ni:

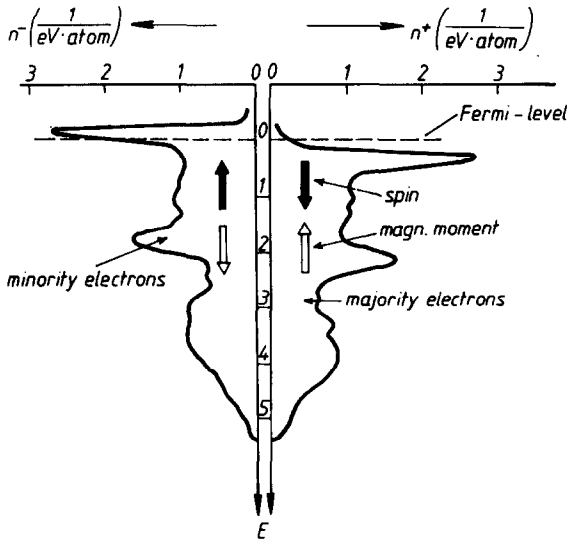


Fig. 10. Spin-polarized total electron densities for Ni as function of electron energy E according to Hodges, Ehrenreich and Lang [81].

1. Fermi electrons exhibit a predominance of minority-spin electrons ($P < 0$) contrary to the total polarization (magnetization) of the (3d, 4s-p)-electrons which is of majority-spin type ($P > 0$).

2. The magnitude of the polarization of the Fermi electrons is drastically larger than the total polarization P_{tot} of all (3d, 4s-4p)-electrons.

For Ni we get for the ESP of Fermi electrons (fig. 10)

$$P = (n^+(E_F) - n^-(E_F)) / (n^+(E_F) + n^-(E_F)) = -67\% \quad (19)$$

and for the total ESP (fig. 10 [81])

$$P_{tot} = (n^+ - n^-) / (n^+ + n^-) = +5.6\%. \quad (20)$$

We remark that one of the most striking features of the SSW theory, the existence of a high minority-ESP for Fermi electrons, refers to an evaluation of the ESP from spin-polarized electron densi-

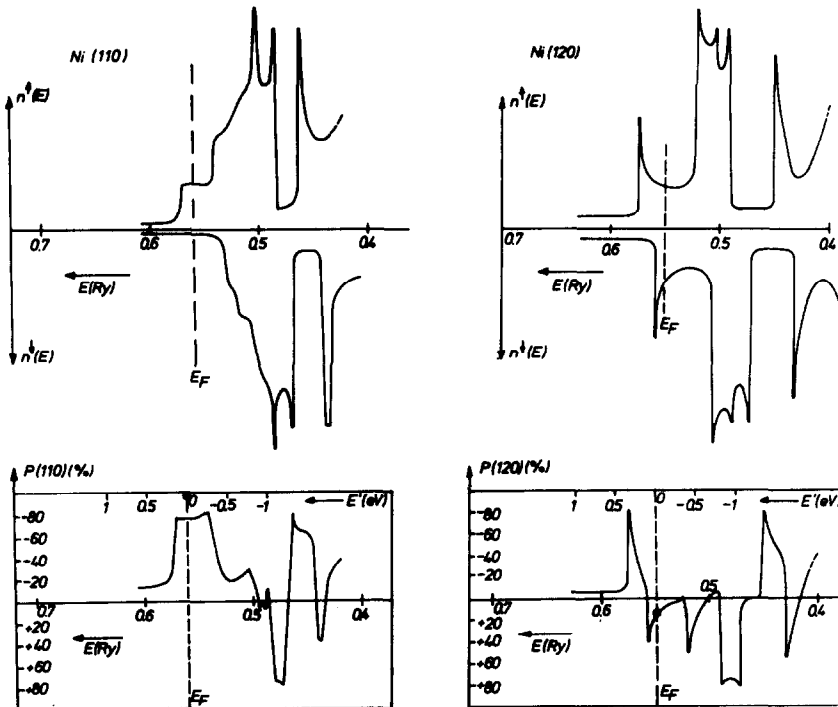


Fig. 11. One-dimensional spin-polarized electron densities (upper part) and (hkl) -dependent electron spin polarization (lower part) as function of electron energy E for Ni(110), Ni(120) as evaluated from band structures by Marshall and Bross [88]. (Black dots: $P(hkl)$ data from ECS experiments using OEC.)

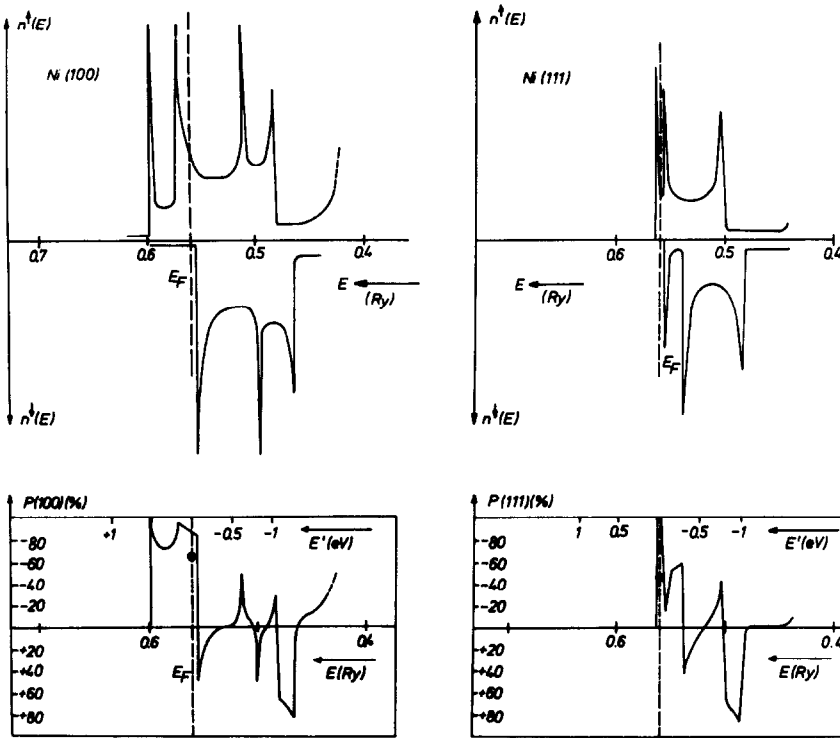


Fig. 12. One-dimensional spin-polarized electron densities and ESP for Ni(100) and Ni(111) [88]; cf. fig. 11).

ties of state integrated over-all directions in k -space.

In the following we deduce a (hkl) -dependent ESP taking into consideration the symmetry directions in k -space which are related to each (hkl) -surface.

In figs. 11 and 12 one-dimensional spin-polarized electron densities of state for Ni(110), Ni(120), Ni(100) and Ni(111) are plotted which are graphically evaluated from band-structure calculations [88]. In addition we have plotted, in figs. 11 and 12, the ESP as a function of the surface indices (hkl) and electron energy E

$$P(hkl, E) = \frac{(n_{hkl}^+(E) - n_{hkl}^-(E))}{(n_{hkl}^+(E) + n_{hkl}^-(E))}. \quad (21)$$

In the frame of testing the applicability of bulk band-structure calculations for the interpretation of ECS measurements at single-crystalline surfaces (table 2, $d_{\min} = 0.2$ nm), the following assumptions are made:

The exponential tail of the electron density at the surface where the electron-capture takes place is populated – in a first simple classical approximation using the itinerant electron picture – with the most weakly bound electrons which are electrons with maximum kinetic energy (Fermi electrons) with k -vectors normal to the reflecting (hkl) -surface.

We note that beside this qualitative argument it

Table 3
Comparison of Ni-ESP data for Fermi electrons as deduced from band structure [88] and from ECS measurements using OEC

(hkl)	Band structure [88] (%)	Experiment (%)
110	- 81	- 96
100	- 94	- 65
111	- 75	- 44
120	+ 17	+ 16

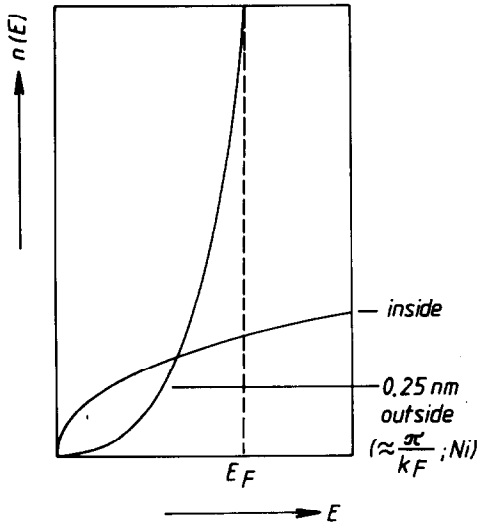


Fig. 13. Local density of states for electrons inside the bulk and ≈ 0.25 nm outside the surface of normal metals treated within the “planar uniform background model by Werner, Schulte and Bross [99].

is, for normal metals, also quantitatively shown in the frame of the “planar uniform background”-model that the width of the energy distribution of occupied electronic states decreases with increasing distance from the surface. The maximum of these local electron densities lies at the Fermi level [99] (fig. 13). This behaviour should be also valid for surfaces of transition metals.

Table 3 gives a comparison of (hkl) -dependent experimental ESP data for Ni from ECS measurements in comparison with ESP values for Fermi electrons taken from figs. 11 and 12.

Comparing the theoretical $P(hkl)$ values with the experimental $P(hkl)$ data there is a complete agreement with respect to the sign of $P(hkl)$ and a rough accordance with respect to the magnitude of the different $P(hkl)$ values.

We have evaluated (hkl) -dependent ESP data for Fermi electrons from all bulk band structure calculations for Ni available from the literature and listed in the last column of table 2. For all band structures there is complete agreement with respect to the sign of the ESP. The small fluctuations between the theoretical $P(hkl)$ data for Ni deduced from various band structure calculations are note-worthy, revealing the high standard of

quality Ni band structure calculations have reached. This statement naturally is related to electron properties at the Fermi level. Restricting ourselves to evaluate only theoretical $P(hkl)$ values from band structures where the ferromagnetic exchange splitting is k -dependent, then these fluctuations are further reduced towards the experimental $P(hkl)$ data. This perfect agreement concerning the sign of the $P(hkl)$ results suggests – at least for Ni – that the magnetic structure calculated in the frame of one-electron band calculations for infinitely extended materials is not drastically changed by the introduction of a surface. This statement naturally is related to the energy region near the Fermi level and confirms the theoretical proposals of Desjonqueres and Cyrot-Lackmann [74] (see section 3.1).

We remark that from ECS measurements performed at atomically clean and flat single-crystalline Ni surfaces, experimental data of Liebermann and coworkers [100], measured at polycrystalline surfaces of Ni where magnetically dead layers are found, cannot be verified.

3.2.2. Cobalt

At room temperature Co has a hcp lattice structure. Among the 3d-ferromagnetic materials Co has received least attention. Contrary to Ni and Fe the status for Co of theoretical investigations is much less advanced. According to Wohlfarth [101] hcp-Co also can be regarded as a typical itinerant electron ferromagnet tractable within the frame of the SSW-model.

Deducing ESP from spin-polarized electronic densities of state integrated over all k -directions, a high minority-ESP of Fermi electrons is postulated contrary to the low majority-ESP (+17%) of all magnetic electrons [91]. The comparison of the different band-structure calculations [91–93] shows that the magnitude of the ferromagnetic exchange splitting (1.1–3.1 eV), as well as the position of the Fermi level, are not accurately known, leading to large uncertainties with respect to the ESP of the Fermi electrons, which is also visible from the large spread of the theoretical $P(hkl)$ data for hcp-Co, derived analogous to Ni from one-dimensional, spin-polarized electron densities of state (see table 2).

ECS results using OEC at surfaces of hcp-Co single crystals are shown in table 2. The three surface directions investigated so far all yield an ESP unequal to zero, therefore excluding the existence of magnetic dead layers at these surfaces contrary to the experimental results of Liebermann and coworkers [100] measured at polycrystalline Co surfaces.

These ECS measurements reveal – in accordance with the Ni results – a drastic dependence of the ESP on surface orientation. For two surfaces ((10 $\bar{1}$ 0), (11 $\bar{2}$ 0)) the experiment yields a majority-ESP and for the Co(0001) surface an ESP of minority-type.

Comparing the $P(hkl)$ data derived from bulk band-structure calculations with the ECS results using OEC yields agreement for only two surfaces ((10 $\bar{1}$ 0) and (0001)) with respect to the sign of ESP. We remark, however, that for hcp-Co more refined ferromagnetic band structure calculations for the bulk – and naturally also for surfaces – must be awaited allowing the estimation of changes in the magnetic structure caused by surface effects.

3.2.3. Iron

ECS measurements using OEC at oriented

single-crystalline surfaces of bcc Fe exhibit ESP values (see table 2) unequal to zero, a fact which analogous to Ni and Co surfaces excludes the existence of magnetic dead layers at these surfaces [100].

On the basis of the ESP results given in table 2 it is evident that for Fe-surfaces the ESP also depends on surface orientation.

For Fe there exist only a few bulk band structures. They are calculated on the basis of the SSW-model [94–98].

P_{tot} for Fe is of majority-type (+28%) and the ESP of the Fermi electrons averaged over all k -directions amounts to approximately +50% [95].

Theoretical $P(hkl)$ values for Fe are given in table 2. They are derived from spin-polarized, one-dimensional electron densities of state for Fe utilizing the available bulk band structure calculations and using the same evaluation method as for Ni and Co.

From table 2 we see that for the (100) and (110) surfaces of Fe there is agreement with respect to the sign of ESP.

Inspection of the various band structure calculations reveals that there exist considerable differences concerning the magnitude of the ferro-

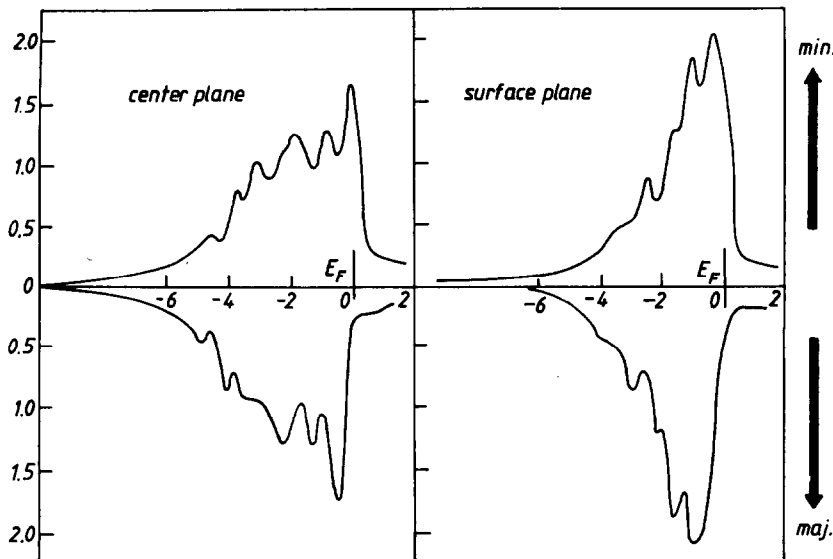


Fig. 14. Self-consistent planar, spin-polarized electron densities for the center plane and the surface plane of Ni(100): Electrons/(eV atom spin) as function of electron energy E in eV according to Wang and Freeman [80]. In the upper part the minority-spin densities, and in the lower part the majority-spin densities are plotted.

magnetic exchange splitting (1.3–3.9 eV) leading to uncertainties with respect to the position of the Fermi level and consequently to uncertainties with respect to the $P(hkl)$ values of the Fermi electrons.

According to photoelectronic measurements by Pessa, Heimann and Neddermeyer [102], performed at single crystalline surfaces of Fe, it is conceivable that the Fermi level with respect to the d-states is positioned 0.6 eV too high in the band structure for ferromagnetic Fe published by Singh, Wang and Callaway [94]. Taking this assumption into consideration there is for all three Fe-surfaces, investigated so far, complete agreement with respect to the sign of the respective $P(hkl)$ values.

3.3. Surface states: Ni(100)

The existence of surface states (SS) is strongly correlated with the structural and electronic properties of a surface [103]. At an ideal periodic surface nonlocalized SS can exist. In addition localized SS can be generated by perturbations in the periodicity (adsorbed impurity atoms, atomic steps, point defects, surface reconstruction) of the atoms at the surface [104]. These states can cause nonlocalized SS to change or to disappear. Therefore a relevant attachment of theoretical to experimental data needs the exact knowledge of the geometrical and chemical structure of the topmost atomic layers of a surface.

According to Wang and Freeman (WF) [80] theoretically reliable proposals on the existence of SS, in principle, require a self-consistent calculation of the surface potential. Caruthers and Kleinman [105] derive from their calculations on the influence of different nonself-consistent potentials on SS at ideal periodic Fe(100)-surfaces, that particularly for layers of transition metals self-consistency is necessary, since the existence and symmetry of SS extremely depend on the details of the potential.

Quite recently it has become possible to calculate self-consistently spin-polarized electron densities of states for oligatomic single crystalline layers including SS, a most promising fact which henceforth allows one to focus attention on possible changes in the magnetic structure going from

the bulk to the surface which are derived solely from theoretical investigations.

In first ab-initio, self-consistent calculations on spin-polarized electron densities of state (DOS) for a 9 layers thick Ni(100) film, the influence of nonlocalized SS on the ESP at the surface is investigated [80]. These calculations neither yield a magnetic dead layer at the Ni(100) surface nor generate a change in sign of P at the Ni(100) surface. WF find majority-SS at the Fermi level which reduce the minority-ESP of Fermi electrons from -78% (center plane) to -57% (surface plane). These ESP data are deduced from the spin-polarized planar DOS which are shown in fig. 14.

ECS measurements, using OEC at the surface of a 7 layers thick single-crystalline Ni(100) film epitaxially grown on a NaCl(100) substrate crystal, yield an ESP of -64% (see section 3.5) in close agreement with the ESP measured at surfaces of bulk Ni(100) which amounts to -64% (table 2).

Comparing ECS results for Ni(100) with spin-polarized, self-consistent surface band-structure calculations there is not only agreement with respect to the sign of $P(100)$ but also good accordance with respect to the magnitude of $P(100)$.

We note that at present there exists no calculation on the dependence of P as function of distance from the topmost atomic surface sheet. We remark that the P data from ECS experiments using a reflection angle of 0.2° are related to a minimum distance of the ions from the surface of approximately 0.2 nm.

3.4. Dependence of ESP on reflection angle: Ni(110), Co(0001)

Changing the reflection angle α of the ions opens the way to probe surface magnetic structures in real space.

An increase of α enlarges the energy E_{\perp} of the ions normal to the reflecting surface and leads therefore to a decrease of d_{\min} , the distance of closest approach of the ions during the surface reflection (see eq. (18) and fig. 9).

Table 4 lists ECS data using OEC at Ni(110) and Co(0001) surfaces as function of α , E_{\perp} and d_{\min} which are received, increasing α from 0.2 to

Table 4
Dependence of ESP on reflection angle α

Reflection angle α (deg)	Transverse energy E_{\perp} (eV)	Ni(110)		Co(0001)	
		P (%)	d_{\min} (nm)	P (%)	d_{\min} (nm)
0.2	1.8	-96	0.18	-41	0.21
0.5	11.4	+5	0.07	-40	0.11
0.8	29.2	+9	0.03	+21	0.06

0.8° [106,107]. A characteristic feature of these measurements is that for these surfaces there is not only a change in the magnitude of P with increasing α , but also a transition from minority-type ESP to majority-type ESP.

At present there exist no calculations on the local DOS of ferromagnetic surfaces as function of distance from the topmost surface sheet. We proceed to discuss these ECS results in the frame of bulk band-structure calculations using the following assumptions: With increasing α (decreasing d_{\min}) the ions not only probe electrons with wave vectors normal ($k_{\perp} \neq 0, k_{\parallel} = 0$) to the surface but also electrons with k -vectors oblique ($k_{\perp} \neq 0, k_{\parallel} \neq 0$) to the surface lying within a cone of angle ϵ which enlarges with increasing α (fig. 15).

For Ni(110) a calculation on the dependence of ESP on cone angle ϵ is available [106] giving a change of $P(110)$ from -80% (small ϵ) to $+9\%$

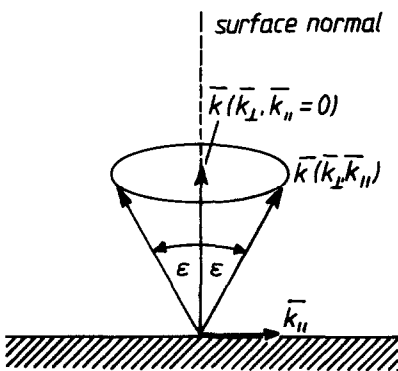


Fig. 15. Cone angle ϵ for electron \bar{k} vectors at the surface. ϵ decreases with increasing distance from the surface (see also text and ref. [3]), k_{\perp} and k_{\parallel} are the vector components of \bar{k} normal and parallel to the surface.

(large ϵ), in good agreement with the experimental finding. For the evaluation of these ESP values the energetic position of the Fermi level in the band-structure calculation is shifted to lower energies by 0.2 eV, which is conceivable as mentioned by the authors [88] if spin orbit coupling would be taken into account.

3.5. Ferromagnetism at surfaces of oligatomic epitaxial Ni(100)-layers

In past years much experimental and theoretical work has been centered upon the electronic and magnetic properties of thin films of ferromagnetic materials [5]. In particular experiments by Liebermann and coworkers [100] stimulated the discussions on magnetic phenomena in thin films. These authors measured the magnetization of thin polycrystalline electrolytically prepared Fe, Co and Ni films as function of film thickness and concluded on the basis of their experimental results that "intrinsically magnetic dead layers" exist at surfaces of 3d-transition metals. For Ni, e.g., they found that until a film thickness of 4 atomic layers is reached, the magnetization at room temperature remains zero. With increasing layer thickness this "dead layer" effect did not disappear. Using different substrate crystals (Cu, Au) they could exclude the possibility that these dead layers could be introduced by diffusion of substrate atoms into the ferromagnetic films.

For theoretical work on the interpretation of these measurements we refer to section 3.1.

Based on experimental facts [108-110] Gradmann [111] pointed out that this effect may be induced by H-chemisorption during the electrolyti-

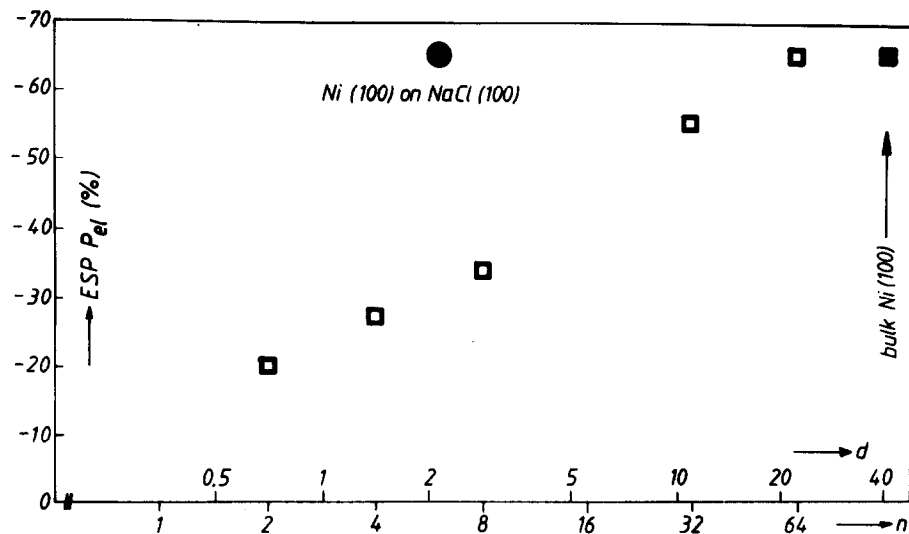


Fig. 16. ESP at surfaces of n monolayers Ni(100) on Cu(100) substrate crystals (open squares), measured with ECS at room temperature using OEC (d = layer thickness in nm). ESP of 7 monolayers Ni(100) and NaCl(100) bulk substrate crystals (closed circle); ESP at surfaces of bulk Ni(100) crystals (closed square).

cal preparation of these films and may be not present at clean surfaces of these metals. Therefore ESP measurements performed under UHV conditions at atomically clean and flat surfaces are very desirable [111].

For ECS experiments atomically clean and flat Ni(100) films (2–64 layers) are prepared on Cu(100) and NaCl(100) substrate crystals by electron beam evaporation at 1×10^{-9} mbar. The absence of holes in these oligatomic is checked by measuring AES signals as a function of layer thickness [112,113] and the monocrystalline state of the surfaces is detected by LEED.

Fig. 16 gives experimental results for the ESP measured with ECS using OEC at surfaces of thin Ni(100) layers. The measurements are performed at room temperature. The ESP at the surface of two atomic layers Ni(100) on Cu(100) amounts to -19% clearly excluding the existence of so-called “intrinsic magnetic dead layers” at Ni(100) surfaces. Increasing the thickness of the Ni(100) layers on Cu(100) up to 64 layers increases the ESP up to -65% close to the ESP value (-64%) measured at surfaces of bulk Ni(100). Note that the decrease of ESP with decreasing Ni-layer thickness cannot be attributed to a decrease of the bulk Curie temperature T_{Cb} because it is known

from reliable UHV experiments [114,115] that T_{Cb} does not depend on layer thickness, at least down to a layer thickness of 2 nm (6 atomic layers).

In a further experiment, 7 atomic layers Ni(100) are evaporated on NaCl(100) substrate crystals. The ESP at these surfaces amounts to -64% (fig. 16) and is not reduced compared to the Ni(100)/Cu(100) experiment where, e.g., 8 monolayers Ni(100) on Cu(100) yield an ESP of -33% . Therefore the observed reduction of the ESP at the free Ni(100) surface using Cu(100) substrate crystals might be caused by the influence of non-polarized Cu-substrate electrons, which due to electron-phonon scattering at room temperature have a mean free path of approximately 2–4 nm [116].

Unfortunately, at present, there exists no detailed calculation on the ESP at surfaces of thin Ni(100) layers on Cu(100) substrate crystals as a function of Ni-layer thickness.

We note, however, that a self-consistent calculation – including SS – on the magnetic structure of a 9 layer thick *unsupported* Ni(100) is available [80]. The ESP at the surface of this film amounts to -57% which is close to the ESP at the surface of 7 atomic layers Ni(100) on NaCl(100) which amounts to -64% . These authors (WF) note that

for films of thickness less than 7 layers there is also a dependence of the ESP on layer thickness for unsupported films.

Quite recently, Freeman and coworkers [117] investigated the surface magnetism of one Ni overlayer on a five layer Cu(100) substrate. They find a reduction of the surface-ESP of Fermi electrons caused by the Cu-substrate, which is in agreement with the experimental ECS results.

3.6. Magnetic surface phase transitions: Gd

The influence of a surface on magnetic phase transitions has been investigated by a large number of authors within the framework of different theoretical models [118–124]. There is considerable interest in experimental information on the temperature dependence of the surface magnetic structure. Highly desirable are measurements near the critical temperature.

One of the reasons for lack of experimental data is that it is not so easy to prepare clean surfaces which remain uncontaminated and well-defined during multiple heating and cooling cycles which are necessary to get reliable information.

Under the ferromagnetic metals the rare earth metal Gd, which has a critical temperature around room temperature, seems to be a good candidate because at room temperature bulk impurity diffusion is negligible and undesirable residual gas adsorption during the heating and cooling cycles is negligible under extreme UHV conditions.

Gd is a nearly isotropic ferromagnetic metal with a saturation magnetization of $7.55\mu_B$ /atom where $7\mu_B$ /atom are attributed to the 7 localized electrons in the half-filled 4f-shell and $0.55\mu_B$ /atom are due to the polarization of the 5d–6s conduction electrons, which analogous to the transition metals have a high DOS near the Fermi level. In the framework of the Rudermann–Kittel–Kasuya–Yosida (RKKY) theory [125] it is assumed that the alignment of the magnetic moments of the 4f-electrons is generated by the indirect interaction via the conduction electrons. It is known from neutron diffraction experiments [126] that the polarization of the conduction electrons $P(T, H)$ is proportional to the reduced magnetiza-

tion $m(T, H)$ of the 4f-electrons. We therefore set [127]:

$$P(T, H) = \gamma m(T, H). \quad (22)$$

Sign and magnitude of γ depend on the spin-polarized DOS near the Fermi level.

Fig. 17 gives ECS results utilizing OEC for the ESP measurements at surfaces of polycrystalline bulk Gd magnetized in a magnetic field $H = 47.76$ kA/m. The dashed line in fig. 17 shows the temperature dependence of the bulk magnetization of Gd for $H = 47.76$ kA/m [128]. The ESP at clean (C and O content within the 4 topmost atomic layers is less than 1/100 monolayer as detected by AES) Gd surfaces amounts to -41% at $T = 160$ K and decreases to -4.6% at $T = 293$ K, which is 0.5 K beyond the bulk Curie temperature $T_{Cb} = 292.5$ K measured in situ by an inductive method. At $T = 393$ K zero ESP is found.

Three interesting aspects of this measurement [129] are to be noted:

1. The existence of a nonzero ESP below T_{Cb} agrees well with the RKKY theory and with ferromagnetic band structure calculations of Harmon and Freeman [130] which predict a minority-ESP of Fermi electrons for all calculated low-index (hkl) surface orientations.

2. The temperature dependence of the ESP at

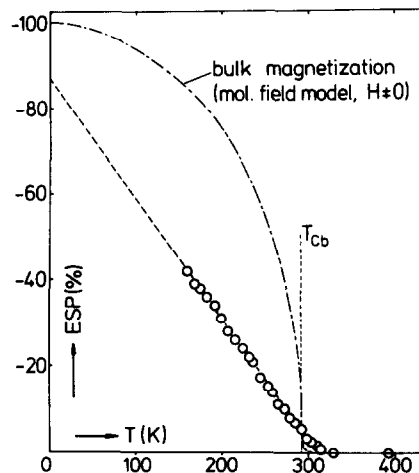


Fig. 17. ESP at Gd surfaces as function of temperature T measured in a magnetizing field of 47.76 kA/m with ECS using OEC.

the topmost surface layer is drastically different from bulk behaviour. Between 160 K and 311 K the ESP changes *linearly* with temperature.

3. $P \neq 0$ above T_{Cb} shows that the surface Curie temperature $T_{Cs} \approx 311$ K is beyond T_{Cb} indicating that the surface layer has a highly anisotropic exchange where the surface coupling constant is larger than the bulk exchange coupling constant [127,130a]. To this we remark that a change of the lattice constant at the surface by a few percent already could increase the magnetic exchange constant by a factor of two.

3.7. H-chemisorption and surface magnetism

The investigation of H-chemisorption at surfaces of 3d-transition metals is of actual interest for the understanding of catalytical processes. Differences in the catalytic properties of these metals can be ascribed to differences in the filling of the d-bands which influence the strength of the adsorptive bonding of H at the surface [131].

H-chemisorption experiments under extreme UHV conditions are of crucial importance for an unsophisticated interpretation of experimental results on the SMO of magnetic metals where the hydrogen partial pressure in the measuring chamber is unknown [100]. In an ECS experiment using OEC at a Ni(110) surface it is shown [132] that hydrogen adsorption influences SMO. The ESP at Ni(110) is found to be reduced from -96% at the clean surface to -8% for a hydrogen coverage at the surface of approximately one monolayer. This directly reveals that H-chemisorption induces magnetically dead layers which do not exist at the uncontaminated surface. At present there exist several promising theoretical investigations where it is shown that an antiferromagnetic interaction between the chemisorbed H atoms and the substrate atoms gives rise to a change of the SMO [132a-d].

3.8. Surfaces of antiferromagnetic 3d-transition metals: Cr(100)

The 3d-metal Cr is antiferromagnetic below the

bulk Néel temperature $T_{Nb} = 310$ K and consists of two magnetically compensating ferromagnetic sublattices producing zero macroscopic magnetization of the bulk. In the (100)-direction the spin structure is sinusoidal and incommensurate with the lattice period. Therefore one might expect ferromagnetic order at the topmost surface layer of Cr(100) below T_{Nb} .

The Cr(100) crystal used in the measurements is prepared with a surface orientation better than 0.01° . After several standard cleaning-annealing procedures the final C and O coverages are less than 0.02 monolayer as monitored with AES using a CMA. LEED measurements at the surface of the clean and atomically flat Cr(100) single crystal show a $c(2 \times 2)$ surface structure.

The ESP is investigated with ECS using OEC [39]. Increasing the applied magnetic field up to 0.09 T an ESP up to $-(18 \pm 2)\%$ is found at $T = 293$ K clearly revealing the existence of long-range ferromagnetic order at the topmost atomic layer of Cr(100) $c(2 \times 2)$. With increasing temperature the ESP decreases to $-(2.5 \pm 1)\%$ at 310.5 K for $B = 0.09$ T. Linear extrapolation yields zero ESP for $B = 0$. At 365 K zero ESP is detected for all applied magnetic fields.

At present there is one calculation available where within a simple tight-binding approximation it is shown that the nonreconstructed Cr(100) surface is already ferromagnetic [133]. Teraoka and Kanamori [134], Werner [135] and Gempel [135a] derive that magnetic order at Cr surfaces may also exist beyond T_{Nb} . Work is in progress to measure the ESP near T_{Nb} with high precision.

We remark that quite recently in a further interesting experiment [135b] oxygen-induced ferromagnetism at a nitrogen-stabilized (N coverage < 1 monolayer on top of the surface) nonreconstructed Cr(100) $p(1 \times 1)$ surface is observed with spin-polarized photoemission spectroscopy (see section 4.1). In this experiment the topmost 2 nm of the surface are probed. At $T = 230$ K the maximum ESP amounts to $+9\%$ for a Cr sample containing 3.3% oxygen incorporated below the topmost surface layer. At $T \geq 500$ K the ESP vanishes.

Table 5
Experimental data on the ESP at Ni surfaces

<i>(hkl)</i>	ECS			OEC <i>P</i> (%)	PES <i>P</i> (%)
	TEC				
	$R_{Ni} \times 10^3$	$R_{Cu} \times 10^3$	$ P $ (%)		
(110)	0.35	5.70	94	-96	-95 ^a
(100)	1.45	5.25	72	-64	-30 ^b
(111)	3.05	5.75	47	-45	-45 ^c
(120)	4.62	-	14 ^d	+15	-
polycr.	-	5.37 ^d			

^{a-d} Refs. [136-139].

3.9. Local magnetic order and two electron capture (TEC): Ni(110), Ni(100), Ni(111), Ni(120)

First experiments with ECS for the investigation of TEC processes were performed on demagnetized Ni(110) surfaces. From table 2 we see that the (110)-surface of Ni at $T = 293$ K exhibits an ESP of -96% using OEC (measurement of "long-range" SMO) showing that the tail of the electron density at this surface overwhelmingly (98%) consists of electrons of one spin direction only.

Reflecting 100 keV deuterons at Ni(110) and Cu(110) surfaces at $T = 293$ K drastically different charge state ratios are obtained. $R_{Cu}(110)$ amounts to 5.7×10^{-3} whereas $R_{Ni}(110)$ amounts only to 0.35×10^{-3} . From eq. (17) we get $|P_{Ni}(110)| = 94\%$ which is close to the ESP measured with OEC showing that TEC experiments open a simple new way to investigate SMO.

The results of further systematic studies [39] at various Ni(*hkl*) surfaces are listed in table 5 together with OEC data. From the comparison of the respective ESP values we see that the evalua-

Table 6
Experimental results on the electron spin polarization *P* (%) measured at various surfaces of clean and H-adsorbed Ni

<i>(hkl)</i>	PES	FES	SIFT	ECS
110	-95 (1980) [148]	-8 (1971) [155] +3 (1975) [152]; H ₂ : +2.2 +5 (1978) [160]; H ₂ : +1.2		-96 (1975) [13]
100	-30 (1976) [137]	-10 (1971) [155] 0 (1977) [157]; H ₂ : +15 -3 (1977) [158]; H ₂ : 0		-65 (1975) [13]
111	-45 (1979) [138]	+7.5 (1971) [155] -3.5 (1977) [157]; H ₂ : +15		-44 (1975) [13]
120		+3.6 (1976) [156]		+16 (1975) [13]
137		-9.5 (1971) [155]		
130		+3.6 (1976) [156]		
112		-2.9 (1976) [156]		
113		-2.9 (1976) [156]		
123		+7 (1977) [159]		
poly-cryst.	+15 (1970) [145]	-13 (1971) [155]	+11 (1972) [165]	

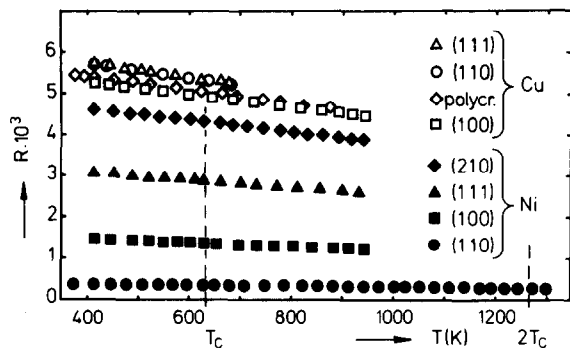


Fig. 18. Charge-state ratios $R_{Ni}(hkl)$ and $R_{Cu}(hkl)$ as function of the target temperature T . Polycr. refers to polycrystalline Cu. For Ni only each second measuring point is drawn in order to give a clear plot.

tion of $|P|$ as given by eq. (17) is useful in determining SMO although at present a proper theoretical treatment of TEC for grazing-angle reflection experiments is not available [38]. We have further listed in table 5 data on the ESP at Ni(hkl) surfaces measured with spin-polarized photoemission spectroscopy (PES) which are in good agreement with the ECS results.

In fig. 18 measurements on the temperature dependence of the “local” SMO at various Ni and Cu surfaces are shown. From fig. 18 we see that there is no drastic increase of the $R_{Ni}(hkl)$ data near T_{Cb} as one would expect in a conventional picture of ferromagnetism where, as a result of the disappearance of the ferromagnetic exchange splitting beyond T_{Cb} – assuming that T_{Cs} is near T_{Cb} – the SMO should disappear.

The ECS results shown in fig. 18 suggest that “local” ferromagnetic order exists on an atomic scale within atomic neighbours for Ni far above the Curie temperature, e.g., for Ni(110) up to $2.05T_{Cb}$, implying that the “local” ferromagnetic exchange splitting is temperature independent as stated in modern theories where the finite temperature properties of the 3d-transition metals are treated in the frame of a “local band” picture where the interatomic exchange produces ferromagnetism [140–143]. We remark that Slater [65] in 1968 already pointed out that there is no interrelation between the ferromagnetic exchange splitting and the Curie temperature, which is characterized only by the disappearance of the long-

range spin order, whereas the energy separation between minority- and majority-spin electrons is correlated with exchange effects existing on an atomic scale.

4. Results of further experimental techniques sensitive to ESP at magnetic surfaces

As mentioned in section 1.2 the aim of this review is not to give an extended description – except ECS – of the various ESP methods. We will limit ourselves to describe the different techniques insofar as necessary to comprehend the principle of each method and report on recent advances and developments as they relate to new and fundamental results in the years past which have brought new scientific perspectives in surface magnetism research. Until recently, experimental results on ESP at ferromagnetic surfaces measured with different techniques seemed to be conflicting. By way of example we report on ESP data on Ni, which has been investigated with all methods.

The interpretation of the ESP data from ferromagnetic Ni (see table 6) where the SMO has been probed with ECS, PES (spin-polarized photoemission spectroscopy), FES (spin-polarized field-emission spectroscopy) and SIFT (spin-dependent tunneling in a superconductor–insulator–ferromagnet junction), lead to contradictory conclusions concerning the applicability of the SSW band theory to describe ferromagnetism in the 3d-transition metals [5–10,13,23]. The center of the controversies was the interpretation of the different signs of the ESP measured with each method at Ni-surfaces.

Each method not only provides information on the magnetic state of the surfaces but also information on the understanding of the physical processes inherently involved in each technique. Moreover, new information and insights can be obtained by advances in the experimental technique, e.g., in PES experiments presently specimens magnetized along the surface plane can also be successfully investigated.

Rapid computational progress these days allows the development of powerful arithmetic techniques to carry out complicated calculations which are necessary to determine the magnetic and electronic

structure of surfaces. These advances in the past few years have lead to a limitation of the large number of possible models to describe magnetism at surfaces.

At his point we would like to mention a further interesting field: investigation of surface magnons from light scattering experiments. A recent review that includes this area is published by Lévy [143a].

4.1. Photoemission spectroscopy (PES)

Single photon absorption by electrons in a ferromagnetic solid leads to the emission of spin-polarized electrons. The ESP predominantly is detected using the well-known Mott detector. The mean free path of photoelectrons amounts to approximately 1–3 nm. Since the emission time of photoelectrons ($< 10^{-14}$ s) is much smaller than the spin relaxation time (10^{-12} s) in solids, it is assumed that during the emission process the ESP remains unchanged.

After the first unsuccessful results in 1965 on Ni-surfaces [144], Siegmann and coworkers showed in their pioneering experiments in 1970 that it is possible to detect ESP at surfaces of polycrystalline evaporated Ni, Co and Fe films [145,146]. For the ESP of electrons near the Fermi level they found:

Ni: +15%, Co: +28%, Fe: +54%.

In these measurements the energy resolution at the Fermi level amounted to 400 meV.

A characteristic for Ni was the positive sign of the ESP which consequently – according to this measurement – lead to the inapplicability of the SSW model (see section 3.1) for the interpretation of the experimental PES-results for Ni. The authors mention that the ESP values found are larger than the expected values for P_{tot} (eq. (20)) deduced from the SSW model:

Ni: +5%, Co: +19%, Fe: +28%.

In 1976 for the first time a minority-ESP was found at surfaces of single-crystalline Ni(100) where inhomogeneities in the work function, always present at polycrystalline surfaces, can be avoided [147]. We note that this interpretation by the authors is in accordance with ECS data known

from the $P(hkl)$ data for Ni (table 2 see also figs. 11 and 12) where Ni(120), which possesses the lowest work function compared to other low-index Ni-surfaces, yields a positive ESP. Therefore at polycrystalline Ni surfaces one would expect at photothreshold a positive ESP neglecting thereby any other effects. Later on for Ni(111) a negative ESP at the Fermi level was also found [147,138].

We remark that up till 1979 the specimens used in PES experiments were magnetized normal to the surface (longitudinal geometry) in consideration of electron optical requirements. New and outstanding experimental data now have been received with samples magnetized along the surface (transversal geometry) and without applying a magnetizing field during the measurements [136]. For Ni(110) an ESP at the Fermi level of -95% was found by making use of optical selection rules.

The investigation of the SMO at single-crystalline surfaces of Ni at present yields the following maximum values for the photo-ESP at the Fermi level:

Ni(<i>hkl</i>)	:	(110)	(111)	(100)
<i>P</i> (%)	:	-95	-45	-30

We remark that these photo-ESP data naturally depend on the energy resolution at the photothreshold [148].

For a recent review on this field we refer to ref. [149] and to ref. [150] where the authors deduce from their PES-experiments that the one-electron band picture cannot be used for the interpretation of the found data on the photo-ESP below the Fermi level.

Finally, we also note that from conventional PES experiments applying optical selection rules valuable information on various physical properties of ferromagnetic materials, such as the temperature dependence of the ferromagnetic exchange splitting, can be received [150a–c].

4.2. Fieldemission spectroscopy (FES)

By applying a high electric field at a tip of a ferromagnetic solid the potential barrier at the surface changes drastically thereby leading to emission of polarized electrons into vacuum. The

main contribution to the emission current originates from electrons near (100 meV) the Fermi level. The ESP is – analogous to the PES experiment – detected using a Mott detector.

The investigation of a (*hkl*)-dependent ESP in field emission experiments requires extreme experimental efforts [151] concerning:

1. the vacuum conditions for measurements at low temperatures (< 100 K),
2. the adjustment of the electric and magnetic field device,
3. the precise selection of the emission current originating from the different (*hkl*)-surface orientations [152].

For static magnetic fields larger than 0.5 T and for electrical extraction fields larger than 2.5 keV the disturbance of the field emission pattern is too large to allow a (*hkl*)-dependent investigation of the ESP [151]. We remark that for the interpretation of FES experiments drastic differences in the transmission coefficients for tunneling of d-like electrons (T_d) and for sp-like electrons (T_{sp}) must be taken into account ($T_{sp} \approx (10-100)T_d$) [153,154].

First FES experiments on polycrystalline Ni-tips were reported in 1971 by Gleich and coworkers [155]. They found an ESP of -13% . They further reported on a minority-ESP for electrons emitted around (100), (110), (137) and on a majority-ESP for electrons emitted around (111). In 1975 Müller [152] reported on a change in the sign of the ESP induced by H-adsorption.

In years past, series of new FES-data were achieved by the further development of the experimental technique [152,156–160]. Due to the large number of experimental results they are summarized in table 6. Note that in the publications [158,160] for Ni(100) and Ni(110) only a reduction of the FES-ESP is found but no change in the sign by adsorbing hydrogen at the Ni-tips. In ref. [157], on the other hand, an increase of the ESP up to $+15\%$ is found for Ni(100) and Ni(111), which for Ni(111) is associated with a change in the sign of the FES-ESP. Further clarification of this situation needs experimental data on the influence of CO adsorption on the ESP at Ni surfaces. We note that Eib [161] from preliminary experiments finds an increase of the ESP caused by CO adsorption.

Further complication for the interpretation of FES experiments arises from a possible spin-dependence of the surface potential. This spin-filter effect is of importance for the interpretation of FES-ESP data from Ni and Fe as claimed in a theory published by Nagy [162].

4.3. Spin-dependent tunneling in a superconductor–insulator–ferromagnet junction (SIFT)

The basis of the SIFT method is related to the spin-dependence of energy states of quasiparticles in thin superconducting Al-films in high magnetic fields [163]. In first experiments using Al–Al₂O₃–Ni layers, the spin dependence of the tunneling current is reported [164–167].

The preparation of the films [166] is performed by evaporating a 5 nm thick Al layer on a glass substrate at $T = 77$ K in a vacuum of 10^{-5} mbar followed by an oxidation of the Al-layer for 4 h at room temperature in air saturated with water vapour. After this procedure a 30–100 nm thick Ni layer is evaporated in vacuum on the Al₂O₃ surface. The measurement of the tunnel characteristic is performed at 0.4 K in a magnetic field of 3.4 T. With SIFT spin-polarized electron densities within an energy width of 0.001 eV near the Fermi level can be probed. For the interpretation of the measurements it is assumed that the tunneling process does not depend on spin direction [164]. Polycrystalline Ni, Co and Fe yield the following SIFT-ESP values which are all of majority-spin type [166,167]:

Ni: $+11\%$, Co: $+34\%$, Fe: $+44\%$.

The authors exclude the applicability of the SSW model for the interpretation of the SIFT results. In a further paper they point at the high surface sensitivity of this method [167].

From further investigations using Ni–Fe, Ni–Mn, Ni–Ti, Ni–Cr, Ni–Cu alloy layers they deduce a strong correlation between the measured ESP and the respective magnetic moment of these alloys [168,169] and consequently they also exclude, on principle, the applicability of the SSW-model for the interpretation of SIFT data measured for 3d-transition metal alloys [170,7]. SIFT experiments on the SMO of ultrathin layers of

ferromagnetic materials revealed that for Fe [171] at 0.4 K 2 atomic layers are already ferromagnetic contrary to measurements for Ni where for Ni layers of thickness less than 3 atomic layers no ferromagnetic behaviour is found [172].

We remark that work is in progress to perform SIFT experiments under UHV conditions at ferromagnetic surfaces where the surface orientation is known [173].

4.4. Diffraction of spin-polarized low-energy electrons (SPLEED)

Diffraction of spin-polarized electrons at magnetic surfaces opens a most promising way to achieve information on the surface magnetic properties of ferro- and antiferromagnetic materials. At present two comprehensive and extensive reviews [11,12] on SPLEED are published which concentrate on various aspects of theoretical and experimental SPLEED-research at surfaces of magnetic and nonmagnetic materials.

We will limit ourselves to report on recent pioneering SPLEED-experiments performed at surfaces of ferromagnetic 3d-transition metals. First, investigations on the spin dependence of polarized electron scattering using Ni(110) surfaces were reported by Celotta et al. [174] and Pierce et al. [175].

In these experiments polarized electrons from a GaAs source are diffracted at the 2 topmost atomic layers of a Ni(110) crystal magnetized parallel to the surface plane to reduce depolarization effects caused by stray magnetic fields, which are already small if a magnetic shunt is provided for the magnetic flux [175]. The intensity and the scattering asymmetry of the diffracted specular beam is measured using a Faraday cup and a polarization modulation technique coupled with phase-sensitive detection [12]. The authors find from their experimental data on Ni(110) that the surface magnetization changes – within the temperature region $0.5 \leq T/T_{Cb} \leq 0.8$ – linearly with temperature which is drastically different from bulk behaviour. Work is in progress to perform SPLEED experiments on surfaces of Fe(110) [177].

Recently, Alvarado et al. [178] reported on the magnetic critical behaviour at Ni(100) surfaces

near T_{Cb} . They find from the evaluation of their experimental data in the temperature range $0.008 \leq 1 - T/T_{Cb} \leq 0.1$, that the surface magnetization decreases with the critical exponent $\beta_1 = 0.825$ which possibly indicates XY coupling at the Ni(100) surface. We remark that they also find from their experiment that for this surface T_{Cb} is equal to T_{Cs} to within ± 4 K. The above reported experiments indicate that SPLEED is a powerful tool of great future potential for the investigation of surface magnetic properties.

We remark that in recent successful experiments by Siegmann et al. [179] on the spin-dependent absorption (inelastic scattering) of electrons in a ferromagnetic metal, new and efficient principles for simple ESP detectors were discovered.

Finally, we note that the first experiments in the field of studying magnetism with electron diffraction were performed by Palmberg and co-workers [179a] who showed that conventional LEED can be used to study antiferromagnetism, since the antiferromagnetic unit cell is twice the size of the chemical unit cell.

5. Summary and perspectives

As discussed in this review there has been strong progress in fundamental research on the SMO of ferromagnetic metals. In the past few years a large amount of mutually competing information on SMO of ferromagnetic metals under UHV conditions has been achieved with different experimental techniques. For a critical examination of the advantages and limitations of the five experimental techniques sensitive to SMO we have focused attention on experimental results for Ni, which is generally recognized to play a key role for testing the applicability of theoretical models on ferromagnetism.

ECS is a technique for magnetic surface analysis with extreme sensitivity in real space. With ECS the long-range SMO, and in addition the “local” SMO existing at the topmost atomic layer of a magnetic material, can be investigated. Utilizing two-electron capture processes in ECS, “local” SMO existing at an atomic scale within atomic neighbours can be investigated without applying

any magnetizing field, which can be of crucial importance for measurements where the critical behaviour of ferromagnets near phase transitions is explored. ECS has been applied to a number of ferromagnetic materials to investigate interesting phenomena. As a result, many questions concerning surface magnetism have been answered using present-day knowledge about the physics of ECS. With ECS studies it is shown that only well-defined and atomically clean surfaces of single crystals reflect the magnetic and electronic properties of the material in consideration, a fact which has high-lighted the importance of single crystal measurements. Ni(*hkl*) surfaces, e.g., exhibit high ESP values which directly reveals that band-structure calculations treated in the framework of the SSW model are not fundamentally inadequate to account for the ground-state surface magnetic properties of ferromagnetic metals; no so-called intrinsic magnetic dead layers could be observed at clean surfaces. We note, however, if the original clean surface is contaminated with one monolayer of hydrogen the ESP drops to zero showing the disappearance of ferromagnetism at the surface. This was found by ECS and FES UHV experiments. With ECS it is further shown that two atomic layers of Ni already are ferromagnetic, which is of considerable interest for testing theoretical models.

Measurements on the temperature dependence of the long-range SMO at Gd surfaces show drastic differences compared to the magnetic behaviour of the bulk, a finding most important for the promotion of prevailing theoretical notations. Experiments on the "local" SMO at Ni(*hkl*) surfaces show that "local" ferromagnetic order at Ni surfaces exist far above T_{Cb} , for Ni(110) up to $2T_{Cb}$ suggesting that spin-split bands may be maintained at these high temperatures. In further ECS studies it is shown that the reconstructed (100) $c(2 \times 2)$ surface of antiferromagnetic bulk Cr is ferromagnetic. This is detected by ECS in a straightforward way in combination with LEED investigations.

In PES experiments strong recent progress (see table 6) has been achieved by measuring ESP at single crystalline surfaces and by the successful introduction of the "transversal geometry" in PES

where recently optical selection rules are also taken into consideration. We remark that PES is a method of great future potential, which allows us to probe electron states in *k*-space not only at the Fermi level but also far below the Fermi energy. Recent differentially energy-resolved PES results on the ESP of electrons emitted from below the Fermi level reveal that the found photo-ESP cannot be explained within the one-electron band picture. On the other hand, proving the validity of a model where Auger transitions with final localized two-hole bound states are involved the found photo-ESP data can be well understood.

In FES in the past years extreme experimental efforts towards an improvement of the experimental feasibilities have led to new FES-ESP data (see table 6) where the experimental conditions are better known. These FES-ESP data for Ni and Fe can be successfully interpreted in the frame of band structure calculations if a spin dependence of the surface potential is taken into consideration.

SIFT experiments using polycrystalline Ni-, Co- and Fe- layers and also 3d-transition metal alloys yield all ESP values which are of majority-spin type. In the interpretation of their data the authors exclude the applicability of the SSW model. It is conceivable that new refined SIFT-ESP results – performed under UHV conditions at ferromagnetic surfaces where the surface orientation is known – must be awaited for a final conclusion on the inapplicability of the SSW model for the interpretation of the experimental SIFT-ESP data which are known to carry information on the electronic and magnetic properties of electrons within only 1 meV near the Fermi level.

In first most promising SPLEED experiments on single crystalline Ni-surfaces under UHV conditions the temperature dependence of the surface magnetization is investigated and found to depend linearly on temperature. In a further experiment it is demonstrated that SPLEED allows us to determine surface critical exponents with high precision. It is to be expected that SPLEED – on the basis of a close coupling between theory and experiment – will develop into a very powerful technique rendering it possible to obtain information on a layer-dependent surface magnetization. At this point we note that one expects from a recent

theory by Felcher [180] on reflection of polarized, cold (wavelength ≈ 0.5 nm) neutrons at ferromagnetic surfaces that neutrons can be utilized as a probe of surface magnetism with a sensitivity corresponding to one atomic layer. A further contribution in this area is made by Mazur and Mills [180a] who have calculated the inelastic scattering of neutrons by surface spin waves on ferromagnetics.

Quite recently, Gradmann and coworkers [181] developed a UHV magnetometer for the investigation of well-characterized magnetic layers which also will become a powerful tool for answering fundamental questions in magnetism.

The prospects for the future application of SMO-sensitive spectroscopies are highly promising. One topic is related to answer challenging questions in technological important fields such as catalysis and corrosion. How does the SMO change by adsorption and subsequent dissociation of molecules used in heterogeneous catalysis? How are changes in the catalytic activity of a ferro- or antiferromagnetic catalyst reflected in changes of the long-range or the "local" SMO? The answer to these questions will provide a framework towards a comprehensive theory on catalytic processes which presently is not available. It is to be expected that future experiments on SMO will make fundamental contributions in this field. These experiments certainly will include not only pure ferromagnets but also ferromagnetic alloys such as NiCu which are widely used as catalysts. There the relative NiCu composition at the topmost atomic layer easily can be changed by interdiffusion and controlled by AES. ESP analysis then could yield information on the possible reduction of the "local" exchange splitting between minority- and majority-spin electrons with increasing Cu/Ni ratio which is to be expected in the frame of modern band theories. We note that surface treatments such as ion sputtering, oxidation-reduction or temperature treatments change the catalytic activity of the alloy surface by orders of magnitude which might be due to the change in the NiCu composition.

A further topic is related to answer fundamental questions concerning critical phenomena such as phase transitions at surfaces of bulk ferromag-

nets or at adsorbed layers on top of a ferromagnet. One may ask: How are order-disorder transitions of hydrogen chemisorbed on top of single crystalline Ni surfaces correlated with changes in the SMO? Investigations on the change of the SMO below and beyond the Curie or Néel point are of extreme interest for testing temperature-dependent bulk and surface band-structure calculations. At present it is unknown if nonferromagnetic materials such as V and Mn exhibit ferromagnetism if monolayers are deposited on substrate materials with lattice constants different from that of bulk V or Mn. The extension of experiments on SMO towards the investigation of spin glasses or mixed valence systems is of special theoretical interest [62].

We believe that the recent progress in understanding surface magnetism will be accelerated in the near future on the premise of the achievement of a deeper comprehension of the physical processes inherently involved in each method. Further stimulus for surface magnetism research will come from the exploration of new ESP detectors. This promising challenge has widely been recognized and met. In ECS, e.g., detection of two-electron capture processes [39], or polarized-light emission from spin-polarized electron capture into excited atomic states, opens the way for new spin detectors [182]; in SPLEED, e.g., presently in experiments on spin-dependent absorption of electrons in ferromagnetic metals, the use of a new spin detector is being explored [179].

After completing this review we received a theoretical treatment by Jepsen et al. [183] on the spin-polarized electronic structure of unsupported thin Ni(100) films. Graphical evaluation of the ESP for Fermi electrons yields for the center plane of a 5-layer thick Ni(100) film an ESP of -82% which changes by excess states on the surface layer to -75% . From these self-consistent calculations no evidence is found either for magnetic dead layers at the surface or for a change of the sign of the ESP of Fermi electrons at the surface (see sections 3.3 and 3.5).

Acknowledgements

The author of this review is very grateful to his colleagues in surface magnetism research for stimulating and critical questions, clarifying discussions and for sending him theoretical and experimental results prior to publication.

References

- [1] P. Fulde, *Physica* 91B (1977) 251.
I. Peschel and P. Fulde, *Z. Phys.* 259 (1973) 145.
- [2] E.P. Wohlfarth, *Physica* 91B (1977) 305.
- [3] J.A. Appelbaum and D.R. Hamann, *Rev. Mod. Phys.* 48 (1976) 479.
- [4] M.C. Gutzwiller, *AIP Conf. Proc.* 10 (1973) 1179.
- [5] U. Gradmann, *Appl. Phys.* 3 (1974) 161.
- [6] H.C. Siegmann, *Phys. Rep.* 17C (1975) 37.
- [7] R. Meservey, P.M. Tedrow and D. Paraskevopoulos, *AIP Conf. Proc.* 29 (1975) 276.
- [8] M. Campagna, D.T. Pierce, F. Meier, K. Sattler and H.C. Siegmann, in: *Advances in Electronics and Electron Physics*, vol. 41, ed. L. Martin (Academic Press, New York, London, 1976) p. 113.
- [9] R. Sizmann, *Nucl. Instr. and Meth.* 132 (1976) 523.
- [10] T.E. Feuchtwang, P.H. Cutler and J. Schmit, *Surface Sci.* 75 (1978) 401.
T.E. Feuchtwang, P.H. Cutler and D. Nagy, *Surface Sci.* 75 (1978) 490.
- [11] R. Feder, *J. Phys.* C14 (1981) 2049.
- [12] D.T. Pierce and R.J. Celotta, in: *Advances in Electronics and Electron Physics*, vol. 56, ed. C. Marton (Academic Press, New York, 1981).
- [13] C. Rau and R. Sizmann, *Phys. Lett.* 43A (1973) 317; *Atomic Collisions in Solids*, vol. 1, eds. S. Datz et al. (Plenum, New York, 1975) p. 295.
- [14] G.A. Bennet and R.B. Wilson, *J. Sci. Instr.* 43 (1966) 669.
- [15] R.B. Wilson, *J. Sci. Instr.* 44 (1967) 53.
- [16] E. Rabinowicz, *Sci. Am.* 281 (1968) 91.
- [17] R.S. Farago, *Rep. Progr. Phys.* 34 (1971) 1055.
- [18] S.E. Darden, *Am. J. Phys.* 35 (1967) 727.
- [19] J.B.A. England, *Techniques in Nuclear Structure Physics* (Wiley, New York, 1974).
- [20] G. Breit and I.I. Rabi, *Phys. Rev.* 38 (1931) 2082.
- [21] P. Kush and V.W. Hughes, in: *Handbuch der Physik*, vol. 37/1, ed. S. Flügge (Springer, Berlin, 1959) p. 81.
- [22] W. Haerberli, *Ann. Rev. Nucl. Sci.* 17 (1967) 373.
- [23] C. Rau, *Comments on Solid State Phys.* 9 (1980) 177.
- [24] A.S. Davydov, *Quantum Mechanics* (Pergamon Press, Oxford, 1965).
- [25] A. Messiah, *Quantum Mechanics*, Vol. 2 (North-Holland, Amsterdam, 1962).
- [26] *Experimental Nuclear Physics*, ed. E. Segre (Wiley, New York, 1953).
- [27] R.D. Evans, *The Atomic Nucleus* (McGraw-Hill, New York, 1955).
- [28] A. Galonsky, H.B. Willard and T.A. Welton, *Phys. Rev. Lett.* 2 (1959) 349.
- [29] L.J.B. Goldfarb, *Nucl. Phys.* 12 (1959) 657.
- [30] W. Trächslin, H. Bürgisser, P. Huber, G. Michel and H.R. Striebel, *Helv. Phys. Acta* 38 (1965) 523.
- [31] F. Seiler, E. Baumgartner, W. Haerberli, P. Huber and H.R. Striebel, *Helv. Phys. Acta* 35 (1962) 385.
- [32] H. Grunder, R. Gleyvod, G. Lietz, G. Morgan, H. Rudin, F. Seiler and H. Stricker, *Helv. Phys. Acta* 44 (1971) 662.
- [33] H. Rudin, H.R. Striebel, E. Baumgartner, L. Brown and P. Huber, *Helv. Phys. Acta* 43 (1961) 58.
- [34] L.J.B. Goldfarb and A. Huq, *Helv. Phys. Acta* 38 (1965) 541.
- [35] C.L. Pekeris, *Phys. Rev.* 126 (1962) 1470.
- [36] R. Hill, *Phys. Rev. Lett.* 38 (1977) 643.
- [37] Using other ions, e.g. $^4\text{He}^{2+}$, the relative intensities of triplet- He^0 and singlet- He^0 must be measured.
- [38] J.R. Hiskes, *J. de Phys. Colloq.* 40 (1979) C7-179.
- [39] C. Rau and S. Eichner, *Phys. Rev. Lett.* 47 (1981) 939.
- [40] Ch. Kittel, *Introduction to Solid State Physics* (Wiley, New York, 1966) 3rd ed., chap. 15.
- [41] J. Lindhard, *Mat. Fys. Medd. Dan. Vid. Selsk.* 34 (1965) 1.
- [42] D.S. Gemmel, *Rev. Mod. Phys.* 46 (1974) 129.
- [43] R. Sizmann and C. Varelas, in: *Festkörperprobleme XVII*, ed. J. Treusch (Vieweg, Braunschweig, 1977) p. 261.
- [44] L.H. Thomas, *Proc. Camb. Phil. Soc.* 23 (1926) 542.
- [45] E. Fermi, *Z. Phys.* 48 (1928) 73.
- [46] G. Molière, *Z. Naturforsch.* 2a (1947) 133.
- [47] W. Brandt and R. Sizmann, *Phys. Lett.* 37A (1971) 115.
- [48] W. Brandt, in: *Atomic Collisions in Solids*, vol. 1, eds. S. Datz et al. (Plenum Press, New York, 1975) p. 261, and refs. cited therein.
- [49] M.C. Cross, *Phys. Rev. B* 15 (1977) 602, and refs. cited therein.
- [50] M. Kitagawa, K. Koyama and Y.H. Ohtsuki, *Phys. Rev. B* 13 (1976) 4682.
- [51] S. Horiguchi, K. Koyama and Y.H. Ohtsuki, *Phys. Stat. Sol. (b)* 87 (1978) 757.
- [52] H. Schröder, *Nucl. Instr. and Meth.* 194 (1982) 381.
- [53] J. Neufeld and R. Ritchie, *Phys. Rev.* 98 (1955) 1632.
- [54] G. Ertl, *Ber. d. Bunsen-Ges. f. Phys. Chem.* 75 (1971) 967.
- [55] E. Bauer, *Z. Metallkde.* 63 (1972) 437.
- [56] D.R. Penn, *Phys. Rev. B* 13 (1967) 5248.
- [57] P. Braun and W. Färber, *Vak. Techn.* 23 (1973) 7.
W. Färber and P. Braun, *Mikrochim. Acta (Wien) Suppl.* 6 (1975) 391.
- [58] P. Braun, *Vak. Techn.* 28 (1978) 76.
- [59] H.C. Siegmann, M. Campagna, D.M. Edwards, W. Eib, L. Kleinman, R. Meservey, D.R. Penn, C. Rau and R.E. Watson, *Inst. Phys. Conf. Ser.* 39 (1978) 276.
- [60] A.J. Freeman, R. Feder, D.T. Pierce, C. Rau and H.C.

- Siegmann, *J. Magn. Magn. Mat.* 15–18 (1980) 1070.
- [61] C.S. Wang and A.J. Freeman, *J. Magn. Magn. Mat.* 15–18 (1980) 869.
- [62] W. Zinn and S. Methfessel, *J. Magn. Magn. Mat.* 15–18 (1980) 1588.
- [63] W. Heisenberg, *Z. Phys.* 49 (1928) 619.
- [64] F. Bloch, *Z. Phys.* 57 (1929) 545.
- [65] J.C. Slater, *Phys. Rev.* 49 (1936) 537; *Rev. Mod. Phys.* 25 (1953) 199; *J. Appl. Phys.* 39 (1968) 761.
- [66] E.C. Stoner, *Proc. Roy. Soc. A* 154 (1936) 656, A165 (1938) 372, A169 (1939) 339.
- [67] P. Weiss, *J. de phys.* 6 (1907) 661; *Z. Phys.* 9 (1908) 358.
- [68] E.P. Wohlfarth, *Proc. Roy. Soc. A* 195 (1949) 434; *Rev. Mod. Phys.* 25 (1953) 211.
- [69] J. Friedel, *J. Phys.* F3 (1973) 785.
- [70] J. Kanamori, *Progr. Theoret. Phys. (Kyoto)* 30 (1963) 275.
- [71] J. Hubbard, *Proc. Roy. Soc. A* 276 (1963) 238, A277 (1964) 237, A281 (1964) 401; *Proc. Phys. Soc.* 84 (1964) 455.
- [72] T. Moriya, *J. Magn. Magn. Mat.* 14 (1979) 1, and refs. cited therein.
- [73] D.M. Edwards and M. Sakoh, *Phys. Stat. Sol. (b)* 70 (1975) 611.
- [74] M.C. Desjonquères and F. Cyrot-Lackmann, *Solid State Commun.* 20 (1976) 855.
- [75] P. Fulde, A. Luther and R.E. Watson, *Phys. Rev.* B8 (1973) 440.
- [76] H. Takayama, K. Baker and P. Fulde, *Phys. Rev.* B10 (1974) 2022.
- [77] K. Levin, A. Liebsch and K.H. Bennemann, *Phys. Rev.* B7 (1973) 3066.
- [78] R.L. Kautz and B.B. Schwartz, *Phys. Rev.* B14 (1976) 2017.
- [79] G. Allan, *Surface Sci.* 74 (1978) 79.
- [80] C.S. Wang and A.J. Freeman, *Phys. Rev.* B21 (1980) 4585.
- [81] L. Hodges, H. Ehrenreich and N.D. Lang, *Phys. Rev.* 152 (1966) 505.
- [82] J.W.D. Connolly, *Phys. Rev.* 159 (1967) 415.
- [83] E.I. Zornberg, *Phys. Rev.* B1 (1970) 244.
- [84] B.A. Politzer, *Diss. Pennsylv. State Univ.* (1971) unpublished.
- [85] J. Langlais and J. Callaway, *Phys. Rev.* B5 (1972) 124.
- [86] J. Callaway and C.S. Wang, *Phys. Rev.* B7 (1973) 1096.
- [87] C.S. Wang and J. Callaway, *Phys. Rev.* B9 (1974) 4897.
- [88] E. Marschall and H. Bross, *Phys. Stat. Sol. (b)* 90 (1978) 241.
- [89] S. Wakoh and J. Yamashita, *J. Phys. Soc. Japan* 19 (1964) 1342.
- [90] S. Wakoh, *J. Phys. Soc. Japan* 20 (1965) 1894.
- [91] S. Wakoh and J. Yamashita, *J. Phys. Soc. Japan* 28 (1970) 1151.
- [92] S. Ishida, *J. Phys. Soc. Japan* 33 (1972) 369.
- [93] F. Batallan, I. Rosenman and C.B. Sommers, *Phys. Rev.* B11 (1975) 545.
- [94] M. Singh, C.S. Wang and J. Callaway, *Phys. Rev.* B11 (1975) 287.
- [95] S. Wakoh and J. Yamashita, *J. Phys. Soc. Japan* 21 (1966) 1712.
- [96] K.J. Duff and T.P. Das, *Phys. Rev.* B3 (1971) 192.
- [97] R.A. Tawil and J. Callaway, *Phys. Rev.* B7 (1973) 4242.
- [98] J. Callaway and C.S. Wang, *Phys. Rev.* B16 (1977) 2095.
- [99] C. Werner, F.K. Schulte and H. Bross, *J. Phys. C8* (1975) 3817.
- [100] L.N. Liebermann, D.R. Fredkin and H.B. Shore, *Phys. Rev. Lett.* 22 (1969) 539.
- L. N. Liebermann, J. Clinton, D.M. Edwards and J. Mathon, *Phys. Rev. Lett.* 25 (1970) 232.
- [101] E.P. Wohlfarth, *J. Appl. Phys.* 41 (1970) 1205.
- [102] M. Pessa, P. Heimann and H. Neddermeyer, *Phys. Rev.* B14 (1976) 3488.
- [103] S.G. Davison and J.D. Levine, in: *Solid State Physics*, vol. 25, eds. F. Seitz et al. (Academic Press, New York, 1970).
- [104] M. Henzler, in: *Advances in Solid State Physics*, ed. O. Madelung (Pergamon, Vieweg, Braunschweig, 1971) p. 187.
- [105] E. Caruthers and L. Kleinman, *Phys. Rev. Lett.* 35 (1975) 738.
- [106] S. Eichner, C. Rau and R. Sizmann, *Inst. Phys. Conf. Ser.* 39 (1978) 269.
- [107] S. Eichner, C. Rau and R. Sizmann, *J. Magn. Magn. Mat.* 6 (1977) 204.
- [108] H.J. Bauer, D. Blechschmidt and M. v. Hellermann, *Surface Sci.* 30 (1972) 701.
- [109] P.W. Selwood, *Chemisorption and Magnetism* (Academic Press, New York, 1971).
- [110] G.A. Martin and B. Imelik, *Surface Sci.* 42 (1974) 157.
- [111] U. Gradmann, *J. Magn. Magn. Mat.* 6 (1977) 173.
- [112] M.A. Seah, *Surface Sci.* 32 (1972) 703.
- [113] C.C. Chang, *Surface Sci.* 48 (1975) 9.
- [114] C.A. Neugebauer, *Phys. Rev.* 116 (1959) 1441.
- [115] H. Hoffmann, *Z. Angew. Phys.* 13 (1961) 149.
- [116] H. Ehrenreich, H.R. Philipp and D.J. Olechna, *Phys. Rev.* 131 (1963) 2469.
- [117] D.-S. Wang, A.J. Freeman and H. Krakauer, *Phys. Rev.* B24 (1981) 1126.
- [118] D.L. Mills, *Phys. Rev.* B3 (1971) 3887.
- [119] K. Binder and P.C. Hohenberg, *Phys. Rev.* B6 (1972) 3461.
- [120] R.A. Weiner, *Phys. Rev.* B8 (1973) 4427.
- [121] H.H. Chen and C.S. Hsue, *J. Phys. C7* (1974) 4104.
- [122] K. Binder and P.C. Hohenberg, *Phys. Rev.* B9 (1974) 2194.
- [123] J. B. Sokoloff, *J. Phys. F5* (1975) 1946, 528.
- [124] T. Takeda and H. Fukujama, *J. Phys. Soc. Japan* 40 (1976) 925, 41 (1976) 762.
- [125] M.A. Ruderman and C. Kittel, *Phys. Rev.* 96 (1954) 99.
- T. Kasuya, *Progr. Theoret. Phys.* 16 (1956) 45, 58.
- K. Yosida, *Phys. Rev.* 106 (1957) 893.
- [126] R.M. Moon, W.C. Koehler, J.W. Cable and H.R. Child, *Phys. Rev.* B5 (1972) 997.
- [127] J.S. Helman, private communication.
- [128] H.E. Nigh, S. Legvold and F.H. Spedding, *Phys. Rev.* 132 (1963) 1092.

- [129] C. Rau and S. Eichner, in: Nucl. Phys. Meth. in Mat. Research, eds. K. Bethge et al. (Vieweg, Braunschweig, 1980) p. 354; and to be published.
- [130] B.N. Harmon and A.J. Freeman, Phys. Rev. B10 (1974) 1979. B.N. Harmon, J. de Phys. Colloq. C5 (1979) 65.
- [130a] S. Selzer and N. Majlis, to be published.
- [131] G. Wedler, in: Chem. Text Book, vol. 9 (Chem. Press, Weinheim, 1970).
- [132] S. Eichner, C. Rau and R. Sizmann, J. Magn. Magn. Mat. 6 (1977) 208.
- [132a] H. Kranz, Phys. Rev. B20 (1979) 1617.
- [132b] H. Kranz and A. Griffin, J. Phys. F 10 (1980) 1195.
- [132c] J.E. Ure, E.V. Anda and N. Majlis, Surface Sci. 99 (1980) 689.
- [132d] J.L. Morán-López and L.M. Falicov, J. Vac. Sci. Techn., in press.
- [133] G. Allan, Surface Sci. 74 (1978) 79.
- [134] Y. Teraoka and J. Kanamori, Inst. Phys. Conf. Ser. 39 (1978) 588.
- [135] S.A. Werner, Bull. Am. Phys. Soc. 25 (1980) 182.
(a) D.R. Grempel, Phys. Rev. B24 (1981) 3928.
(b) F. Meier, D. Pescia and T. Schriber, Phys. Rev. Lett. 48 (1982) 645.
- [136] E. Kisker, W. Gudat, E. Kuhlmann, R. Clauberg and M. Campagna, Phys. Rev. Lett. 45 (1980) 2053.
- [137] W. Eib and S.F. Alvarado, Phys. Rev. Lett. 37 (1976) 444.
- [138] E. Kisker, W. Gudat, M. Campagna, E. Kuhlmann, H. Hopster and I.D. Moore, Phys. Rev. Lett. 43 (1979) 966.
- [139] For the evaluation of $|P_{Ni}(120)|$ we have used $R_{Cu}(\text{polycr.})$ because no Cu(120) crystal was available.
- [140] H. Capellmann, J. Phys. F4 (1974) 1466.
- [141] J.B. Sokoloff, Phys. Rev. Lett. 31 (1973) 1417.
- [142] V. Korenmann, J.L. Murray and R.E. Prange, Phys. Rev. B16 (1977) 4032, 4049, 4058.
- [143] T. Moriya, J. Magn. Magn. Mat. 14 (1979) 1.
(a) J.C.S. Lévy, Surface Sci. Rep. 1 (1981) 39.
- [144] R.L. Long Jr., V.W. Hughes, J.S. Greenberg, I. Ames and R.L. Christensen, Phys. Rev. A138 (1965) 1630.
- [145] U. Baenninger, G. Busch, M. Campagna and H.C. Siegmann, Phys. Rev. Lett. 25 (1970) 585.
- [146] G. Busch, M. Campagna and H.C. Siegmann, Phys. Rev. B4 (1971) 746.
- [147] W. Eib and S.F. Alvarado, Phys. Rev. Lett. 37 (1976) 444.
- [148] W. Gudat, E. Kisker, E. Kuhlmann and M. Campagna, Phys. Rev. B22 (1980) 3282.
- [149] E. Kisker, M. Campagna, W. Gudat and E. Kuhlmann, in: Festkörperprobleme (Advances in Solid State Physics), vol. XIX, ed. J. Treusch (Vieweg, Braunschweig, 1979) p. 259.
- [150] R. Clauberg, W. Gudat, E. Kisker, E. Kuhlmann and G.M. Rothberg, Phys. Rev. Lett. 47 (1981) 1314.
(a) W. Eberhardt, E.W. Plummer, K. Horn and J. Erskine, Phys. Rev. Lett. 45 (1980) 273.
(b) D.E. Eastman, F.J. Himpfel and J.A. Knapp, Phys. Rev. Lett. 40 (1978) 1514.
(c) D.E. Eastman, F.J. Himpfel and J.A. Knapp, Phys. Rev. Lett. 44 (1980) 95.
- [151] M. Landolt, priv. communication.
- [152] N. Müller, Phys. Lett. 54A (1975) 415.
- [153] B.A. Politzer and P.A. Cutler, Phys. Rev. Lett. 28 (1972) 1330.
- [154] J.W. Gadzuk, Phys. Rev. 182 (1969) 416.
- [155] W. Gleich, G. Regenfus and R. Sizmann, Phys. Rev. Lett. 27 (1971) 1066.
- [156] M. Campagna, T. Utsumi and D.N.E. Buchanan, J. Vac. Sci. Tech. 13 (1976) 193.
- [157] G. Chrobok, M. Hofmann, G. Regenfus and R. Sizmann, Phys. Rev. B15 (1977) 429.
- [158] M. Landolt and M. Campagna, Phys. Rev. Lett. 38 (1977) 663, 39 (1977) 568.
- [159] M. Landolt, M. Campagna, J.-N. Chazaviel and Y. Yafet, Physica 91B (1977) 96.
- [160] M. Landolt, Y. Yafet, B. Wilkens and M. Campagna, Solid State Commun. 25 (1978) 1141.
- [161] W. Eib, private communication.
- [162] D. Nagy, Surface Sci. 90 (1979) 102.
- [163] R. Meservey, P.M. Tedrow and P. Fulde, Phys. Rev. Lett. 25 (1970) 1270.
- [164] P.M. Tedrow and R. Meservey, Phys. Rev. Lett. 26 (1971) 192.
- [165] R. Meservey and P.M. Tedrow, Solid State Commun. 11 (1972) 333.
- [166] P.M. Tedrow and R. Meservey, Phys. Rev. B7 (1973) 318.
- [167] P.M. Tedrow and R. Meservey, Solid State Commun. 16 (1975) 71.
- [168] R. Meservey, D. Paraskevopoulos and P.M. Tedrow, Phys. Rev. Lett. (1976) 858.
- [169] R. Meservey, D. Paraskevopoulos and P.M. Tedrow, Physica 91B (1977) 91.
- [170] D. Paraskevopoulos, R. Meservey and P.M. Tedrow, Phys. Rev. B16 (1977) 4907.
- [171] R. Meservey, P.M. Tedrow and V.R. Kalvey, Bull. Am. Phys. Soc. 25 (1980) 183.
- [172] R. Meservey, P.M. Tedrow and V.R. Kalvey, Solid State Commun. 36 (1980) 969.
- [173] R. Meservey, private communication.
- [174] R.J. Celotta, D.T. Pierce, G.-C. Wang, S.D. Bader and G.P. Felcher, Phys. Rev. Lett. 43 (1979) 728.
- [175] D.T. Pierce, R.J. Celotta, G.-C. Wang, G.P. Felcher, S.D. Bader and K. Miyano, J. Magn. Magn. Mat. 15-18 (1980) 1583.
- [176] X.I. Saldaña and J.S. Helman, Phys. Rev. B16 (1977) 4948.
- [177] D.T. Pierce, private communication.
- [178] S. Alvarado, M. Campagna and H. Hopster, Phys. Rev. Lett. 48 (1982) 51.
- [179] H.C. Siegmann, D.T. Pierce and R.J. Celotta, Phys. Rev. Lett. 46 (1981) 452.
- [179a] P.W. Palmberg, R.E. DeWames and L.A. Vredevoe, Phys. Rev. Lett. 21 (1968) 682.
- [180] G.P. Felcher, Phys. Rev. B24 (1980) 1595.
- [180a] P. Mazur and D.L. Mills, Phys. Rev. B, to be published.
- [181] R. Bergholz and U. Gradmann, Verhandl. Deut. Phys. Ges. 3 (1981) 300.
- [182] J.C. Tully, N.H. Tolk, J.S. Kraus, C. Rau and R.J. Morris, in: Inelastic Particle-Surface Collisions, Springer Series in Chemical Physics, vol. 17, eds. V.I. Goldanskii et al. (Springer, Berlin, 1981) p. 196.
- [183] O. Jepsen, J. Madson and O.K. Anderson, to be published.